

Article

Microbial weathering of iron-bearing minerals in deep hydrothermally altered granitic rock of a semi-arid environment (Chilean Coastal Cordillera)

C. Schwerdhelm¹ , F. J. Hampl² , L. V. Krone³ , L. Sauter¹, K. Kaphegyi¹, L. Horstmann⁴ , D. Straub⁵ ,
T. Samuels¹ , M. Mansor¹ , C. Merino^{6,7} , F. Matus^{7,8} , F. v. Blanckenburg³ , D. Wagner^{4,9} , T. Neumann¹⁰,
A. Kappler^{1,11} and C. Bryce¹²

¹Geomicrobiology, Department of Geosciences, University of Tübingen, Schnarrenbergstrasse 94–96, 72076 Tübingen, Germany; ²Department of Applied Geochemistry, Technische Universität Berlin, Ernst-Reuter-Platz 1, 10587 Berlin, Germany; now: Chair of Resource Mineralogy, Montanuniversität Leoben, Peter-Tunner-Straße 5, 8700 Leoben, Austria; ³Institute of Geological Sciences, Freie Universität Berlin, Malteserstrasse 74–100, 12249 Berlin, Germany; ⁴GFZ German Research Centre for Geosciences, Section Geomicrobiology, 14473 Potsdam, Germany; ⁵Quantitative Biology Center, University of Tübingen, 72076 Tübingen, Germany; ⁶Center of Plant, Soil Interaction and Natural Resources Biotechnology Scientific and Technological Bioresource Nucleus, Temuco, Chile; ⁷Network for Extreme Environmental Research, Universidad de la Frontera, Temuco, Chile; ⁸Laboratory of Conservation and Dynamics of Volcanic Soils, Department of Chemical Sciences and Natural Resources, Universidad de La Frontera, Temuco, Chile; ⁹University of Potsdam, Institute of Geosciences, Karl-Liebknecht-Str. 24–25, 14476 Potsdam, Germany; ¹⁰Department of Applied Geochemistry, Technische Universität Berlin, Ernst-Reuter-Platz 1, 10587 Berlin, Germany; ¹¹Cluster of Excellence: EXC 2124: Controlling Microbes to Fight Infection, Tübingen, Germany; and ¹²School of Earth Sciences, University of Bristol, Wills Memorial Building, Queens Road, Bristol BS8 1RJ, UK

Abstract

Microbial mineral weathering has been predominantly investigated at shallow depths in humid and tropical environments. Much less is understood about its role in the deeper subsurface of arid and semi-arid environments where microbial weathering is limited by the availability of water and energy sources for microbial metabolism. However, the deep subsurface in these climate zones may host a microbial community that thrives on weathering of iron (Fe)-bearing minerals that serve as electron donors or acceptors.

To investigate the role of microorganisms in weathering of Fe-bearing minerals in a dry climate, we recovered a >80 m deep weathering profile in a semi-arid region of the Chilean Coastal Cordillera. The bedrock is rich in Fe-bearing minerals (hornblende, biotite, chlorite, magnetite and hematite) but lacks detectable organic carbon. We evaluated the bioavailability of Fe(III)-bearing minerals that may serve as an electron acceptor for Fe(III)-reducing microorganisms. Using geochemical, mineralogical and cultivation-based methods, we found enhanced Fe bioavailability and more *in vitro* microbial Fe(III) reduction at increased depth. We obtained an Fe(III)-reducing enrichment culture from the deepest weathered rock found at 77 m depth. This enrichment culture is capable of reducing ferrihydrite (up to 0.6 mM d⁻¹) using lactate or dihydrogen as an electron donor and grows at circumneutral pH. The main organism in the enrichment culture is the spore-forming *Desulfotomaculum ruminis* (abundance of 98.5%) as revealed by 16S rRNA gene amplicon sequencing.

Our findings provide evidence for a microbial contribution to the weathering of Fe-bearing minerals in semi-arid environments. While microorganisms are probably not contributing to the weathering of Fe(II)-bearing silicate minerals, they are most likely of importance regarding reductive dissolution of secondary weathering products. The Fe(III) reduction quantified in this weathering profile by the *in situ* microbial community suggests that microorganisms are active weathering agents in semi-arid climates.

Keywords: Critical Zone; deep weathering; hydrothermal alteration; semi-arid; Fe-metabolising bacteria; Fe(II) oxidation; Fe(III) reduction; sulfate reduction

(Received 08 August 2024; revised 01 January 2025; manuscript accepted: 04 February 2025)

Corresponding author: C. Bryce; Email: casey.bryce@bristol.ac.uk

Cite this article: Schwerdhelm C., Hampl F.J., Krone L.V., Sauter L., Kaphegyi K., Horstmann L., Straub D., Samuels T., Mansor M., Merino C., Matus F., v. Blanckenburg F., Wagner D., Neumann T., Kappler A., & Bryce C. (2025). Microbial weathering of iron-bearing minerals in deep hydrothermally altered granitic rock of a semi-arid environment (Chilean Coastal Cordillera). *Geo-Bio Interfaces* 2, e8, 1–17. <https://doi.org/10.1180/gbi.2025.2>

Introduction

Microbes are active agents in mineral weathering and contribute to the transformation of hard rock to soil in the Critical Zone (CZ) (Ehrlich, 1998; Riebe *et al.*, 2017; Holbrook *et al.*, 2019; Krone *et al.*, 2021b; Hampl *et al.*, 2022). The CZ is defined as Earth's near-surface environment, which regulates life by the interplay of

biological, chemical, physical and geological processes (Brantley *et al.*, 2007). Microbial weathering occurs during all stages of rock–soil transformation from primary rock colonization to rock breakdown and saprolite formation, whereby it also contributes to elemental cycling in the regolith (Banwart *et al.*, 2019; Samuels *et al.*, 2020). Most studies on microbial weathering focus on shallow and humid tropical soils and saprolites or on transects across corestones (Buss *et al.*, 2008; Minyard *et al.*, 2012; Barcellos *et al.*, 2018; Gu *et al.*, 2020). However, much less is understood about the role of microorganisms in weathering processes occurring in the deep (10s to 100s of metres) CZ, especially in (semi-)arid climates where rocks are less intensely weathered (Moser *et al.*, 2003; Fredrickson and Balkwill, 2006; Onstott *et al.*, 2019; Bochet *et al.*, 2020; Takamiya *et al.*, 2021). Furthermore, unlike sedimentary rocks, granitic rocks are a particularly challenging environment for microbial growth because after solidification of hot magma the rocks formed contain neither organic carbon nor cells. Furthermore, because of the lack of microbial weathering studies in the deep subsurface and more arid climates it is possible that we are currently underestimating how quantitatively important and widespread microbial weathering may be.

In such environments, fracturing of rocks is the first process that may enable conditions to form microbial habitats (Pedersen, 1997). Tectonic activity creates fractures on different spatial scales (micrometres to kilometres) that serve as pathways for meteoric water infiltration into the subsurface (Mitchell and Faulkner, 2009). The availability of water throughout all stages of rock–soil transformation is key because water acts as a transport medium for gases such as dissolved O₂ and CO₂ that alter or dissolve soluble minerals, transport organic carbon from the surface to the subsurface and regulate bacterial activity (Brantley *et al.*, 2017). Bacterial activity is not only regulated by the availability of water but also by the presence of elements essential for life (e.g. C, N, P, S) and elements functioning as electron sources and electron acceptors for microbial metabolisms, such as Fe and S of various oxidation states (Napieralski *et al.*, 2019, 2022; Gu *et al.*, 2020).

In dry climatic settings, the supply of meteoric water and thus the O₂, CO₂ and nutrients that are contained in it is limited. Moreover, the available O₂ is readily consumed by abiotic oxidation of Fe(II)-bearing silicates in the upper zone of weathering profiles (White and Yee, 1985; Perez *et al.*, 2005). This weathering process transforms Fe(II)-bearing silicates into secondary phases such as Fe(III) (oxyhydr)oxides and clay minerals. The ensuing volume expansion caused by this transformation generates weathering-induced fractures (Isherwood and Street, 1976; Buss *et al.*, 2005; Bazilevskaya *et al.*, 2015; Kim *et al.*, 2017; Hampl *et al.*, 2022).

The aim of this study was to investigate the role of Fe-metabolising bacteria in the promotion of weathering in a water- and nutrient-deprived system. We investigated an 87.2 m deep weathering profile in granitoid (quartz monzodiorite) rock in a semi-arid region of the Chilean Coastal Cordillera (Santa Gracia [SG]). More specifically, we: (1) identified the presence of Fe(II)-oxidising and Fe(III)-reducing microbes via microbial enrichments; (2) identified the mineralogical and geochemical conditions in which they thrive via Fe extractions and thermodynamic calculations; (3) explored whether they actively induce major weathering by fostering alteration of solids (i.e. via demonstrating active Fe(III) reduction by the *in situ* community); and (4) investigated the *in situ* microbial community composition in the deepest weathering zone via 16S rRNA sequencing. Weathering profile-specific thermodynamic calculations of Gibbs free energy and energy density for chemolithotrophic and organoheterotrophic microbial redox reactions provide constraints for the most favourable metabolic processes (i.e. electron sources) in this deep, arid system.

Materials and methods

Study site

The study was conducted in a semi-arid climate zone of the Coastal Cordillera in Chile, ~18 km northeast of La Serena (Coquimbo) within the Santa Gracia National Reserve. The bedrock of the drilling location (−29.759414°N, −71.160322°E [WGS84]) is a quartz monzodiorite containing biotite (KFe₃AlSi₃O₁₀(OH)₂), chlorite (Fe₅Al₂Si₃O₁₀(OH)₈), hornblende (Fe₇Si₈O₂₂(OH)₂), magnetite (Fe₃O₄) and hematite (Fe₂O₃) (see Table 1) (Krone *et al.*, 2021b). The bedrock is part of granitic to dioritic intrusions of the early Cretaceous (144–124 Ma), fractured by the Atacama Fault Zone and hydrothermally overprinted (Cembrano *et al.*, 2005; Hampl *et al.*, 2022; Trichandi *et al.*, 2022). The study area is characterised by gently dipping hillslopes, mean annual precipitation of <100 mm y^{−1}, mean annual temperature of 16°C and a sparse vegetation coverage of 30–40%, dominated by shrubs and cacti (Ministerio de Obras Públicas de Chile, 2016; Bernhard *et al.*, 2018; Oeser *et al.*, 2018; Oeser and von Blanckenburg, 2020; Übernickel *et al.*, 2020). This semi-arid study site was intensively investigated by geochemical, geophysical and mineralogical methods (Weckmann *et al.*, 2020; Krone *et al.*, 2021b; Hampl *et al.*, 2022; Trichandi *et al.*, 2022) and thus serves as an ideal model site to study microbial contributions to weathering of Fe-bearing minerals from a terrestrial hydrothermally overprinted setting under water- and nutrient-limiting conditions. There are indications of a possible water table in about 68–70 m depth in the form of poor core recovery, a low amplitude zone (acoustic televiewer) and enhanced porosity (up to 9.5%) (Krone *et al.*, 2021b; Hampl *et al.*, 2022), but this is not conclusive evidence due to the lack of *in situ* fluid data. In this study, the term ‘weathering’ in the context of microbial activity includes both the chemical breakdown of primary minerals and the turnover of secondary mineral products, which have been generated by previous hydrothermal events or meteoric weathering.

Drilling procedure and sample preparation

The weathering profile comprises 87.2 m of drilled core, i.e. soil, saprolite and rock. The uppermost 2 m are additionally recovered by a manually sampled soil pit adjacent to the drill hole. Drill core material was obtained by wireline diamond drilling using a PQ3-sized crown and potable water as drill fluid (including contamination control) (Friese *et al.*, 2017; Krone *et al.*, 2021b). After retrieving the drill cores (up to 1.5 m in length), bulk core sample intervals with a length of ~20 cm were aseptically taken using a hammer, a chisel and an angle grinder in the field. Afterwards, the samples were anoxically stored at 4°C. For microbial cultivation, the samples were aseptically split with a rock trimmer and separated into an outer and an inner part in the laboratory. The outer part was further milled to a grain size of <10 μm with a planetary ball mill (used for selective Fe extractions in this study) while the inner part was processed with a disk mill to obtain a grain size of <2 mm (used for all geomicrobiological investigations in this study, i.e. microbial enrichments, ferrihydrite reduction experiments and microbial community sequencing). Samples for geochemical and mineralogical analyses were further ground to a grain size of <63 μm, and an aliquot of both the outer and inner part was taken for contamination control (Hampl *et al.*, 2021; Krone *et al.*, 2021a). Strict contamination control protocols were applied to all samples, which included the use of a tracer in the drill fluid, strict sample handling conditions and the retrieval of inner core samples that had not been in contact with the drill casing, the core liners or the drill fluid (Krone *et al.*, 2021b).

Table 1. Metabolic reactions with minerals investigated in this study. The redox reactions (1–38) represent 14 oxidation and 24 reduction reactions for major Fe minerals identified in the Santa Gracia drill core profile (see Krone *et al.*, 2021b; Hampel *et al.*, 2022). Oxygen or nitrate serve as electron acceptors for microbial Fe(II) oxidation, while dihydrogen or organic carbon (acetate and lactate) serve as electron donors for microbial Fe(III) reduction. The amount of electrons (e^-) transferred per redox reaction (rxn) is listed on the right.

No.	Mineral	Reaction	e^-/rxn ()
<i>Fe(II) oxidation with oxygen as electron acceptor</i>			
1	Magnetite	$4\text{Fe}_3\text{O}_4 + 6\text{H}_2\text{O} + \text{O}_2 \leftrightarrow 12\text{FeOOH}$	4
2	Biotite ¹	$0.1\text{KFe}_3\text{AlSi}_3\text{O}_{10}(\text{OH})_2 + 3.01\text{Mg}^{2+} + 0.755\text{Al}^{3+} + 2.845\text{H}_4\text{SiO}_4 + 0.05875\text{O}_2 \leftrightarrow 1(\text{Mg}_{3.01}\text{Fe}^{2+}_{0.065}\text{Fe}^{3+}_{0.235})(\text{Si}_{3.145}\text{Al}_{0.855})\text{O}_{10}(\text{OH})_2 + 0.1\text{K}^+ + 0.695\text{H}_2\text{O} + 8.185\text{H}^+$	188
3	Biotite ²	$4\text{KFe}_3\text{AlSi}_3\text{O}_{10}(\text{OH})_2 + 12\text{H}_2\text{O} + 16\text{H}^+ + 3\text{O}_2 \leftrightarrow 12\text{FeOOH} + 4\text{K}^+ + 12\text{H}_4\text{SiO}_4 + 4\text{Al}^{3+}$	12
4	Chlorite ¹	$0.08\text{Fe}_5\text{Al}_2\text{Si}_3\text{O}_{10}(\text{OH})_8 + 0.3\text{K}^+ + 1.34\text{Al}^{3+} + 3.76\text{H}_4\text{SiO}_4 + 0.1\text{O}_2 \leftrightarrow 1\text{K}_{0.3}\text{Al}_{1.5}\text{Fe}^{3+}_{0.4}\text{Si}_4\text{O}_{10}(\text{OH})_2 + 2.44\text{H}_2\text{O} + 1.96\text{H}^+$	20
5	Chlorite ²	$4\text{Fe}_3\text{Al}_2\text{Si}_3\text{O}_{10}(\text{OH})_8 + 24\text{H}^+ + 6\text{H}_2\text{O} + 5\text{O}_2 \leftrightarrow 20\text{FeOOH} + 8\text{Al}^{3+} + 12\text{H}_4\text{SiO}_4$	20
6	Hornblende	$4\text{Fe}_7\text{Si}_8\text{O}_{22}(\text{OH})_2 + 74\text{H}_2\text{O} + 7\text{O}_2 \leftrightarrow 28\text{FeOOH} + 32\text{H}_4\text{SiO}_4$	28
7	$\text{Fe}^{2+}_{(\text{aq})}$	$4\text{Fe}^{2+} + 6\text{H}_2\text{O} + \text{O}_2 \leftrightarrow 4\text{FeOOH} + 8\text{H}^+$	4
<i>Fe(II) oxidation with nitrate as electron acceptor</i>			
8	Magnetite	$10\text{Fe}_3\text{O}_4 + 2\text{NO}_3^- + 2\text{H}^+ \rightarrow 30\text{FeOOH} + \text{N}_2$	10
9	Biotite ¹	$0.1\text{KFe}_3\text{AlSi}_3\text{O}_{10}(\text{OH})_2 + 3.01\text{Mg}^{2+} + 0.755\text{Al}^{3+} + 2.845\text{H}_4\text{SiO}_4 + 0.047\text{NO}_3^- \leftrightarrow 1\text{Mg}_{3.01}\text{Fe}^{2+}_{0.065}\text{Fe}^{3+}_{0.235}\text{Si}_{3.145}\text{Al}_{0.855}\text{O}_{10}(\text{OH})_2 + 0.1\text{K}^+ + 0.721\text{H}_2\text{O} + 8.138\text{H}^+ + 0.0235\text{N}_{2(\text{aq})}$	47
10	Biotite ²	$10\text{KFe}_3\text{AlSi}_3\text{O}_{10}(\text{OH})_2 + 42\text{H}_2\text{O} + 46\text{H}^+ + 6\text{NO}_3^- \leftrightarrow 30\text{FeOOH} + 10\text{K}^+ + 10\text{Al}^{3+} + 30\text{H}_4\text{SiO}_4 + 3\text{N}_{2(\text{aq})}$	30
11	Chlorite ¹	$2\text{Fe}_5\text{Al}_2\text{Si}_3\text{O}_{10}(\text{OH})_8 + 7.5\text{K}^+ + 33.5\text{Al}^{3+} + 94\text{H}_4\text{SiO}_4 + 2\text{NO}_3^- \leftrightarrow 25\text{K}_{0.3}\text{Al}_{1.5}\text{Fe}^{3+}_{0.4}\text{Si}_4\text{O}_{10}(\text{OH})_2 + 118\text{H}_2\text{O} + 106\text{H}^+ + \text{N}_2$	10
12	Chlorite ²	$2\text{Fe}_5\text{Al}_2\text{Si}_3\text{O}_{10}(\text{OH})_8 + 14\text{H}^+ + 2\text{H}_2\text{O} + 2\text{NO}_3^- \leftrightarrow 10\text{FeOOH} + 6\text{H}_4\text{SiO}_4 + 4\text{Al}^{3+} + \text{N}_2$	10
13	Hornblende	$10\text{Fe}_7\text{Si}_8\text{O}_{22}(\text{OH})_2 + 178\text{H}_2\text{O} + 14\text{NO}_3^- + 14\text{H}^+ \leftrightarrow 70\text{FeOOH} + 80\text{H}_4\text{SiO}_4 + 7\text{N}_2$	70
14	$\text{Fe}^{2+}_{(\text{aq})}$	$10\text{Fe}^{2+} + 14\text{H}_2\text{O} + 2\text{NO}_3^- \leftrightarrow 10\text{FeOOH} + 18\text{H}^+ + \text{N}_2$	10
<i>Fe(III) reduction with dihydrogen as electron donor</i>			
15	Magnetite	$\text{Fe}_3\text{O}_4 + 6\text{H}^+ + \text{H}_2 \leftrightarrow 3\text{Fe}^{2+} + 4\text{H}_2\text{O}$	2
16	Goethite	$2\text{FeOOH} + 4\text{H}^+ + \text{H}_2 \leftrightarrow 2\text{Fe}^{2+} + 4\text{H}_2\text{O}$	2
17	Hematite	$\text{Fe}_2\text{O}_3 + 4\text{H}^+ + \text{H}_2 \leftrightarrow 2\text{Fe}^{2+} + 3\text{H}_2\text{O}$	2
18	Ferrihydrite	$2\text{Fe}(\text{OH})_3 + 5\text{H}^+ + \text{H}_2 \leftrightarrow 2\text{Fe}^{2+} + 6\text{H}_2\text{O}$	2
19	Biotite ³	$2\text{KFe}^{2+}\text{Fe}^{3+}\text{Si}_4\text{O}_{10}(\text{OH})_2 + 8\text{H}_2\text{O} + 10\text{H}^+ + \text{H}_2 \leftrightarrow 4\text{Fe}^{2+} + 2\text{K}^+ + 8\text{H}_4\text{SiO}_4$	2
20	Biotite ²	$2\text{KFe}^{2+}\text{Fe}^{3+}\text{Si}_4\text{O}_{10}(\text{OH})_2 + 2\text{K}^+ + \text{H}_2 \leftrightarrow \text{K}_2\text{Fe}^{2+}_2\text{Si}_4\text{O}_{10}(\text{OH})_2 + 2\text{H}^+$	2
21	Chlorite ³	$9.09\text{Mg}_{2.89}\text{Fe}^{2+}_{1.78}\text{Fe}^{3+}_{0.22}\text{Al}_{2.49}\text{Ca}_{0.01}\text{Si}_{2.63}\text{O}_{10}(\text{OH})_8 + 156.91\text{H}^+ + \text{H}_2 \leftrightarrow 18.18\text{Fe}^{2+} + 26.27\text{Mg}^{2+} + 0.09\text{Ca}^{2+} + 22.64\text{Al}^{3+} + 23.91\text{H}_4\text{SiO}_4 + 68\text{H}_2\text{O}$	9.09
22	Chlorite ²	$9.09\text{Mg}_{2.89}\text{Fe}^{2+}_{1.78}\text{Fe}^{3+}_{0.22}\text{Al}_{2.49}\text{Ca}_{0.01}\text{Si}_{2.63}\text{O}_{10}(\text{OH})_8 + 0.64\text{Al}^{3+} + \text{H}_2 \leftrightarrow 9.09\text{Mg}_{2.89}\text{Fe}^{2+}_2\text{Al}_{2.56}\text{Ca}_{0.01}\text{Si}_{2.63}\text{O}_{10}(\text{OH})_8 + 2\text{H}^+$	9.09
<i>Fe(III) reduction with acetate as electron donor</i>			
23	Magnetite	$4\text{Fe}_3\text{O}_4 + 23\text{H}^+ + \text{C}_2\text{H}_3\text{O}_2^- \leftrightarrow 12\text{Fe}^{2+} + 12\text{H}_2\text{O} + 2\text{HCO}_3^-$	8
24	Goethite	$8\text{FeOOH} + 15\text{H}^+ + \text{C}_2\text{H}_3\text{O}_2^- \leftrightarrow 8\text{Fe}^{2+} + 12\text{H}_2\text{O} + 2\text{HCO}_3^-$	8
25	Hematite	$4\text{Fe}_2\text{O}_3 + 15\text{H}^+ + \text{C}_2\text{H}_3\text{O}_2^- \leftrightarrow 8\text{Fe}^{2+} + 8\text{H}_2\text{O} + 2\text{HCO}_3^-$	8
26	Ferrihydrite	$8\text{Fe}(\text{OH})_3 + 15\text{H}^+ + \text{C}_2\text{H}_3\text{O}_2^- \leftrightarrow 8\text{Fe}^{2+} + 20\text{H}_2\text{O} + 2\text{HCO}_3^-$	8
27	Biotite ³	$8\text{KFe}^{2+}\text{Fe}^{3+}\text{Si}_4\text{O}_{10}(\text{OH})_2 + 36\text{H}_2\text{O} + 39\text{H}^+ + \text{C}_2\text{H}_3\text{O}_2^- \leftrightarrow 16\text{Fe}^{2+} + 8\text{K}^+ + 32\text{H}_4\text{SiO}_4 + 2\text{HCO}_3^-$	8
28	Biotite ²	$8\text{KFe}^{2+}\text{Fe}^{3+}\text{Si}_4\text{O}_{10}(\text{OH})_2 + 8\text{K}^+ + \text{C}_2\text{H}_3\text{O}_2^- + 4\text{H}_2\text{O} \leftrightarrow 8\text{K}_2\text{Fe}^{2+}_2\text{Si}_4\text{O}_{10}(\text{OH})_2 + 9\text{H}^+ + 2\text{HCO}_3^-$	8
29	Chlorite ³	$72.73\text{Mg}_{2.89}\text{Fe}^{2+}_{1.78}\text{Fe}^{3+}_{0.22}\text{Al}_{2.49}\text{Ca}_{0.01}\text{Si}_{2.63}\text{O}_{10}(\text{OH})_8 + 626.64\text{H}^+ + \text{C}_2\text{H}_3\text{O}_2^- \leftrightarrow 72.73\text{Fe}^{2+} + 105.19\text{Mg}^{2+} + 0.36\text{Ca}^{2+} + 90.55\text{Al}^{3+} + 95.64\text{H}_4\text{SiO}_4 + 268\text{H}_2\text{O} + 2\text{HCO}_3^-$	8
30	Chlorite ²	$36.36\text{Mg}_{2.89}\text{Fe}^{2+}_{1.78}\text{Fe}^{3+}_{0.22}\text{Al}_{2.49}\text{Ca}_{0.01}\text{Si}_{2.63}\text{O}_{10}(\text{OH})_8 + 2.55\text{Al}^{3+} + \text{C}_2\text{H}_3\text{O}_2^- + 4\text{H}_2\text{O} \leftrightarrow 36.36\text{Mg}_{2.89}\text{Fe}^{2+}_2\text{Al}_{2.56}\text{Ca}_{0.01}\text{Si}_{2.63}\text{O}_{10}(\text{OH})_8 + 9\text{H}^+ + 2\text{HCO}_3^-$	8
<i>Fe(III) reduction with lactate as electron donor</i>			
31	Magnetite	$6\text{Fe}_3\text{O}_4 + 34\text{H}^+ + \text{C}_3\text{H}_5\text{O}_3^- \leftrightarrow 18\text{Fe}^{2+} + 18\text{H}_2\text{O} + 3\text{HCO}_3^-$	12
32	Goethite	$12\text{FeOOH} + 22\text{H}^+ + \text{C}_3\text{H}_5\text{O}_3^- \leftrightarrow 12\text{Fe}^{2+} + 18\text{H}_2\text{O} + 3\text{HCO}_3^-$	12
33	Hematite	$6\text{Fe}_2\text{O}_3 + 22\text{H}^+ + \text{C}_3\text{H}_5\text{O}_3^- \leftrightarrow 12\text{Fe}^{2+} + 12\text{H}_2\text{O} + 3\text{HCO}_3^-$	12

(Continued)

Table 1. (Continued)

No.	Mineral	Reaction	e ⁻ /rxn ()
34	Ferrihydrite	12Fe(OH) ₃ + 22H ⁺ + C ₃ H ₅ O ₃ ⁻ ↔ 12Fe ²⁺ + 30H ₂ O + 3HCO ₃ ⁻	12
35	Biotite ³	12KFe ²⁺ Fe ³⁺ Si ₄ O ₁₀ (OH) ₂ + 54H ₂ O + 58H ⁺ + C ₃ H ₅ O ₃ ⁻ ↔ 24Fe ²⁺ + 12K ⁺ + 48H ₄ SiO ₄ + 3HCO ₃ ⁻	12
36	Biotite ²	12KFe ²⁺ Fe ³⁺ Si ₄ O ₁₀ (OH) ₂ + 12K ⁺ + C ₃ H ₅ O ₃ ⁻ + 6H ₂ O ↔ 12K ₂ Fe ²⁺ ₂ Si ₄ O ₁₀ (OH) ₂ + 14H ⁺ + 3HCO ₃ ⁻	12
37	Chlorite ³	54.55Mg _{2.89} Fe ²⁺ _{1.78} Fe ³⁺ _{0.22} Al _{2.49} Ca _{0.01} Si _{2.63} O ₁₀ (OH) ₈ + 939.45H ⁺ + C ₃ H ₅ O ₃ ⁻ ↔ 109.09Fe ²⁺ + 157.64Mg ²⁺ + 0.55Ca ²⁺ + 135.82Al ³⁺ + 143.45H ₄ SiO ₄ + 402H ₂ O + 3HCO ₃ ⁻	12
38	Chlorite ²	54.55Mg _{2.89} Fe ²⁺ _{1.78} Fe ³⁺ _{0.22} Al _{2.49} Ca _{0.01} Si _{2.63} O ₁₀ (OH) ₈ + 3.82Al ³⁺ + C ₃ H ₅ O ₃ ⁻ + 6H ₂ O ↔ 54.55Mg _{2.89} Fe ²⁺ ₂ Al _{2.56} Ca _{0.01} Si _{2.63} O ₁₀ (OH) ₈ + 14H ⁺ + 3HCO ₃ ⁻	12

¹Biotite(bt)/chlorite(chl) → Fe(III) oxides.

²bt/chl → Fe(III) silicates.

³bt/chl → Fe²⁺.

Additionally, fracture covers/fillings of five drill core samples were removed with corundum drill bits to examine their mineralogy in hydrothermally altered zones.

Selective extractions

Selective Fe extractions using hydrochloric acid (0.5 M HCl) and citrate-bicarbonate dithionite (CBD) were performed on samples of the entire weathering profile to quantify the Fe pools available for microbial Fe redox reactions ($N = 59$, technical extraction triplicates). After extraction, Fe(II) and total Fe (Fe(tot)) were spectrophotometrically quantified using the ferrozine assay (Hegler *et al.*, 2008). Furthermore, water-soluble organic carbon and nitrate were extracted to quantify the potentially available amount of these compounds as electron donors and acceptors for microbial Fe(II) oxidation and Fe(III) reduction. Reported dissolved organic carbon and nitrate values were blank corrected. Details of the extractions were as follows:

0.5 M HCl. 0.5 M HCl is considered to extract bioavailable Fe-bearing phases such as ferrihydrite, lepidocrocite, siderite and partly magnetite, maghemite, hematite, goethite, biotite and chlorite via dissolution by protonation (Sidhu *et al.*, 1981; Raiswell *et al.*, 1994; Voelz *et al.*, 2019). We extracted the bioavailable Fe with 0.5 M HCl at room temperature under anoxic conditions in the dark for 24 h, while shaking at 10 rpm (solid:liquid = 1:60) (Roden and Zachara, 1996).

Citrate bicarbonate dithionite. CBD targets reactive Fe minerals such as ferrihydrite, lepidocrocite, akageneite, goethite and hematite via reductive dissolution (Voelz *et al.*, 2019). Extractions were conducted using a solution of 0.27 M trisodium citrate, 0.11 M sodium bicarbonate and 0.1 M sodium dithionite (Lalonde *et al.*, 2012). Samples were extracted in the dark under oxic conditions for 15 min and in a water bath at 75–80°C (solid:liquid = 1:60). The pH of the CBD solution was circumneutral to obtain maximum reduction potential and to avoid precipitation of sulfides.

Water extractions. First, 10 mL of MilliQ water was added to 0.25 g of crushed rock to target water-extractable organic carbon and nitrate. The extract was analysed with a multi N/C 2100S elemental analyser for organic carbon concentrations (Analytik Jena GmbH) via combustion (detection limit = 0.022 mgC g⁻¹ rock). Nitrate in the extracts was analysed with a flow-injection analyser (FIA) using an AA3 HR AutoAnalyser System (Seal Analytical) (detection limit = 0.0002 mgN g⁻¹ rock). Extractions were performed under oxic conditions at room temperature in the dark for 24 h on a shaker (shaking frequency, $f = 180 \text{ s}^{-1}$) (solid:liquid = 1:40).

pH. The potential and active pH of drill core samples were measured as follows: 2 g of milled drill core samples or air-dried soil (<63 μm) were weighed into 15 mL Falcon tubes and either 10 mL of 0.01 M CaCl₂ (potential pH) or 10 mL of MilliQ water (active pH) were added. The Falcon tubes were shaken and the slurries left untouched for 1 h. Thereafter, the Falcon tubes were shaken again and the pH was measured in the supernatant. The procedure was repeated after 24 h to exclude a major shift in pH ($N = 10$, technical extraction triplicates).

Thermodynamic calculations

Based on Fe-bearing silicates and Fe minerals identified in the SG weathering profile (Krone *et al.*, 2021b; Hampl *et al.*, 2022) we calculated the Gibbs energy yields for 38 potential *in situ* chemolithotrophic and organoheterotrophic microbial redox reactions to identify potentially favourable metabolisms (Kappler *et al.*, 2021). Energetic yields are controlled by various factors, such as mineral species, electron donor, electron acceptor, temperature, pH and solute ion concentrations. Oxygen and nitrate served as electron acceptors for microbial Fe(II) oxidation reactions, while dihydrogen or organic carbon (acetate or lactate) served as the electron donor for Fe(III) reduction (Table 1) (see Kappler *et al.*, 2021). Calculations were performed using fixed dissolved ion and gas concentrations, with pH ranging from 6 to 9 based on *in situ* pH values of powdered drill core samples. We compared these Gibbs energy yields with energy density yields (molar vs volumetric Gibbs energy) (Fig. S1), as the latter scales Gibbs energy calculations by the limiting reactant and has been shown to be a more accurate measure for biomass abundance (La Rowe and Amend, 2014; Osburn *et al.*, 2014). Gibbs energy yields were calculated using Eq. 1:

$$\Delta G_r = \Delta G_r^0 + RT \ln Q_r \quad (1)$$

where ΔG_r represents the Gibbs energy of a reaction, R and T represent the gas constant and temperature (in K), respectively, and Q_r represents the activity product. The activity product Q_r can be evaluated from Eq. 2.

$$Q_r = \prod a_i^{v_i} \quad (2)$$

where a_i represents the activity of species i and v_i is its stoichiometric reaction coefficient.

Thermodynamic calculations are based on the geochemical and mineralogical data of the drill core investigated in this study as well as previous studies (Hampl *et al.*, 2021; Krone *et al.*, 2021a). Due to the aridity, the sampling depths and the wireline drilling procedure,

it was not possible to collect *in situ* fluid data. Hence, we also estimated the Gibbs free energy assuming an *in situ* pH of 8 for a range of dissolved ion and gas concentrations. This range included either (1) those typically found in comparable deep biosphere systems (i.e. lower end of ion and gas concentration range) or (2) those that are typically used in laboratory studies and are thus experimentally relevant (Fig. S2) (Bach and Edwards, 2003; Boettger *et al.*, 2013; Heidari *et al.*, 2017; Jones *et al.*, 2018; Xiao *et al.*, 2021). The latter higher concentration condition (2) may also be relevant to a drying period after a rain event because drying increases the concentrations of elements within a microbial biofilm (Table S1).

Microbial enrichments and incubation conditions

Cultivation of microorganisms. Aseptically crushed soil/rock samples were used as inoculum to identify zones of active microbial Fe(II) oxidation and/or Fe(III) reduction ($N = 59$). Fe(II) was provided as an FeS layer in gradient tubes for microaerophilic Fe(II)-oxidising bacteria (three replicates per depth interval). Additionally, Fe(III) was added as synthesized two-line ferrihydrite (Fhy) (as described in Straub *et al.*, 2005) in 96 deep-well plates to test for Fe(III) reduction coupled to acetate/lactate or dihydrogen oxidation (six replicates per depth interval). Under laboratory conditions, the Fe minerals provided were assumed to be bioavailable in addition to the Fe already present in the environmental samples. For inoculation of the native microbial community, crushed core samples were mixed with anoxic mineral medium and added to each setup.

Microaerophilic Fe(II)-oxidising bacteria were grown in gradient tubes following the protocol of Emerson and Floyd (2005), in which we established opposing gradients of oxygen and Fe^{2+} prior to sample injection. Positive growth was indicated by the formation of an orange band (compared to an abiotic control tube = negative control), as exemplified in Lueder *et al.* (2018). As positive control, a microaerophilic Fe(II)-oxidising enrichment culture from a mine (Segen Gottes Mine, southwest Germany) dominated by *Curvibacter* sp. (Picard *et al.*, 2015) from the laboratory culture collection (Geomicrobiology Group, Department of Geosciences, University of Tuebingen, Germany) was used.

To enrich Fe(III)-reducing bacteria, an anoxic mineral medium ($\text{N}_2:\text{CO}_2$ 90:10; see the Supplementary Material for media composition details) was amended with Fhy as an Fe(III) source and either a mix of 5 mM sodium acetate and 5 mM sodium lactate, or H_2 in excess were provided as an electron donor for Fe(III) reduction. Thereafter, the soil/rock slurry was added to 96 deep-well plates which were anoxically incubated for 8 weeks at room temperature in the dark. Positive growth evaluation was based on the formation of black-coloured, reduced Fe(II) minerals in comparison to rusty-orange coloured control wells (Fig. S3). A detailed analysis of the black-coloured minerals can be found in the Supplementary Discussion section. As positive control, the Fe(III)-reducing culture *Geobacter sulfurreducens* (Caccavo *et al.*, 1994) from the laboratory culture collection (Geomicrobiology Group, Department of Geosciences, University of Tübingen, Germany) was used. As Fhy was added as an electron source in addition to the Fe species already present in the environmental samples, control experiments without Fhy were carried out. These control setups included 11 powdered drill core samples to account for background Fe mineral dissolution from the Fe pool of the environmental samples, i.e. by dissolution or microbial Fe(III) reduction. In these control experiments, powdered drill core samples were added to the 96 deep-well plates using

the same media components as for the cultivation experiments, but in contrast did not contain two-line ferrihydrite as an additional Fe(III) source. In this study, *in situ* Fe(III) reduction is defined as the activation of Fe(III)-reducing microbial activity within core samples inoculated into media, as described above.

Fe(III)-reducing enrichments from the eight most promising depth intervals (i.e. those that showed most Fe(III) reduction) were transferred four times each into Hungate tubes ($N = 8$, four biological replicates each) to obtain a robust Fe(III)-reducing enrichment culture. One robust (i.e. healthy and reproducible) Fe(III)-reducing culture was obtained and further characterised as outlined below. For convenience, this Fe(III)-reducing culture is referred to as 'culture SG'.

Ferrihydrite reduction by an enrichment culture

Batch ferrihydrite reduction experiments were conducted to determine which electron donors are used by enrichment culture SG to reduce Fe(III). Experiments were carried out in 58 mL serum bottles filled with 22.5 mL of anoxic 30 mM mineral medium ($\text{N}_2:\text{CO}_2$ 90:10). Biotic setups were amended with 5 mM Fhy as an electron acceptor and (1) 5 mM sodium acetate, (2) 5 mM sodium lactate, (3) a 5 mM sodium acetate/lactate mix, or (4) dihydrogen in excess as an electron donor. The mix of sodium acetate/lactate was used to determine if culture SG (1) can use both electron donors and (2) prefers one over the other. Since we opted not to add inhibitors for sulfate reduction such as molybdate, the sulfate contained in the growth medium could also have served as an alternative electron acceptor. All biotic setups were inoculated with 10% (vol/vol) pre-grown enrichment culture SG. Abiotic setups were identical to biotic setups except for addition of cells to quantify abiotic ferrihydrite dissolution over time. An additional biotic control was set up with Fhy and cells, but without the addition of an electron donor. By doing so, we assessed how much Fe(III) reduction occurs based on the amount of organics carried over from the inoculum. Both biotic and abiotic setups were conducted in triplicate.

Sampling and chemical analysis

For the ferrihydrite reduction experiments, sampling was performed in an anoxic glovebox (100% N_2) by taking an aliquot of 0.6 mL with a needle and syringe (0.55 mm) into a 2 mL Eppendorf tube.

Fe quantification. The sample slurries were anoxically extracted with 6 M HCl for 24 h to target crystalline Fe phases. Fe quantification was conducted via a ferrozine assay (Hegler *et al.*, 2008).

High-pressure liquid chromatography (HPLC). Lactate and acetate were quantified using an HPLC device (Shimadzu) equipped with an Aminex HPX 87H column (BioRad), using a refractive index detector for lactate and a diode array detector for acetate analysis.

Ion chromatography (IC). We quantified the water-extractable sulfate of the rock sample, from which the enrichment culture was obtained, as well as dissolved sulfate in the batch ferrihydrite reduction experiment samples using a Dionex DX-120 ion chromatograph (Thermo).

Raman spectroscopy. Raman spectra of Fe-S minerals within the Fhy microcosms were acquired with an alpha 500R confocal Raman microscope (WITec GmbH). The microscope was equipped with a 532 nm excitation laser, UHTS 300 spectrometer and DV401-BV CCD camera. Optical grating was 600 g mm^{-1} for spectra recording in the range $0\text{--}3790 \text{ cm}^{-1}$, while using a 40× objective with a numerical aperture of 0.6 (EC Epiplan-neofluor, Carl Zeiss). The laser power was adjusted to 0.1 mW using an optical power meter

(PM100D, Thorlabs GmbH). Three spots of each sample were analysed using 10 integrations for 20 s each and combined to create a composite spectrum. Relative intensities were normalised to 100.

Microbial community sequencing

Fe(III)-reducing enrichment culture community compositions

To assess the adaptation of the enrichment culture to the different electron donors provided and its effect on the microbial community composition, DNA was extracted from the cultures after termination of the Fhy microcosms with the DNeasy® PowerSoil® Pro™ Kit (Qiagen). DNA was amplified using forward primer 16S-515F and reverse primer 16S-806R (Caporaso *et al.*, 2011) targeting the V4 region. Library preparation steps (Nextera, Illumina) and 250 bp paired-end sequencing with MiSeq (Illumina) using v2 chemistry were performed by Microsynth AG. Between 1309 and 86,992 read pairs were obtained for each sample (in total 580,028). Samples treated with ferrihydrite and acetate had the lowest read counts (1309, 1312 and 1974), and all other samples had more than 45,000. Sequencing data were analysed with nf-core/ampliseq v2.3.1, which includes all analysis steps and software and is publicly available (Ewels *et al.*, 2020; Straub *et al.*, 2020), with Nextflow v21.10.3 (Di Tommaso *et al.*, 2017) and singularity v3.8.7 (Kurtzer *et al.*, 2017). Primers were trimmed, and untrimmed sequences were discarded (<30% per sample) with Cutadapt version 3.4 (Martin, 2011). Adapter and primer-free sequences were processed with DADA2 v1.22.0 (Callahan *et al.*, 2016) to eliminate PhiX contamination, trim reads (before median quality drops below 35; forward reads were trimmed at 181 bp and reverse reads at 206 bp), correct errors, merge read pairs and remove polymerase chain reaction (PCR) chimeras. Ultimately, 48 amplicon sequencing variants (ASVs) were obtained across all samples. Taxonomic classification was performed with DADA2 and the SILVA v138 database (Quast *et al.*, 2012). Intermediate results were imported into QIIME2 version 2021.8.0 (Bolyen *et al.*, 2019). Five ASVs classified as chloroplasts or mitochondria were removed, totalling <1.7% relative abundance per sample, and retaining 43 ASVs across all samples. Alpha rarefaction curves were produced with the QIIME2 diversity alpha-rarefaction plugin, which indicated that the richness of the samples had been fully observed, except for samples treated with ferrihydrite and acetate.

Native microbial community composition

The community composition of the enrichment was compared to the native (*in situ*) microbial community. Total DNA was extracted from the uncontaminated inner rock core sample (76.5 m depth, IGSN, <https://doi.org/10.60510/GFCHS009N>) using the “DNeasy® PowerSoil® Pro” Kit (Qiagen). Therefore, three replicates containing 1 g of rock powder were weighed into PowerBead Pro Tubes and extracted according to the protocol of the kit manufacturer. During the silica binding step of the extraction, replicates were pooled together to increase DNA concentration. An extraction control was run during all extraction steps to identify potential laboratory and kit contaminants. Microbial community composition was assessed using 16S-rRNA amplicon sequencing with MiSeq (Illumina) with 2 × 300 bp. Library preparation, including polymerase chain reaction and DNA clean-up, was done in the GFZ Potsdam laboratories (Section 3.6 Geomicrobiology). The V4 region of bacterial and archaeal DNA was targeted using the universal primer pair 16S-515F and 16S-806R (Caporaso *et al.*, 2011). During PCR an additional control containing PCR

grade water instead of DNA template was performed to identify PCR contaminants. Barcoded versions of the primers were used to later distinguish between sample, extraction control and PCR control. After successful amplification, the products were purified using the Agencourt AMPure XP PCR Purification Kit (Beckman Coulter) and sent to Eurofins Genomics Germany GmbH (Konstanz, Germany) for sequencing on a MiSeq System. After recovery of the raw data, libraries were demultiplexed using Cutadapt (Martin, 2011). Taxonomic classification was performed using the DADA2 pipeline (Callahan *et al.*, 2016). Reads were truncated (250 forward, 200 reverse) and quality-filtered before the error model was generated. The amplicon sequence variants (ASVs) were assigned to the SILVA taxonomy (Quast *et al.*, 2012). Chloroplast, mitochondria and singletons were removed. The contamination was assessed using the negative controls of the extraction and the PCR run. Potential contaminant sequences were completely removed from the data set, resulting in a total of 25,878 sequences for the investigated rock sample.

Data and statistical analysis

Data analyses were performed in the R statistical environment (R Core Team, 2024) and plots were produced with the package ggplot2 (Wickham, 2016). Fe(III) reduction by *in situ* microbial communities along the SG weathering profile was analysed using a general linear model (LM). We tested the combined effect of electron donor and setup type treatments on Fe(III) reduction (response variable) in a multipredictor model. Setting up the model we included six predictor variables, which can be classified into two experimental variables (electron donor and setup type), two simple environmental variables (bioavailable and crystalline Fe) and two complex environmental variables (depth and alteration). We further added all significant interactions between predictor variables to maximise the variance in Fe(III) reduction values explained by the model. Model assumptions were checked for all selected models and found not to have been violated. For statistical analyses of Fe(III) reduction, all reasonable models were explored and selection based on comparison of differences in the Akaike Information Criterion (Δ AIC) (Zuur *et al.*, 2009). To include all significant interactions while ensuring model parsimony, the best model fit was determined by the dredge() function in the MuMIn package (Barton and Barton, 2015). However, we excluded alteration as predictor variable from our model during the model building process to avoid collinearity (Figs S4–S8). The role of alteration in Fe(III) reduction is still addressed in the discussion. As the general linear model was found to be significant, we ran *post hoc* paired-samples *t*-tests, corrected with Holm’s sequential Bonferroni procedure (Holm, 1979), to assess whether the compared pairs of setup type and electron donor type showed significant differences in mean Fe(III) reduction.

Results

Drill core mineralogy and geochemistry of SG weathering profile

Extractions were performed to quantify the amounts of poorly crystalline and crystalline Fe phases in the drill core samples. Extractions targeted (1) the Fe that is poorly crystalline and prone to be more ‘bioavailable’ to Fe-metabolising microorganisms (via 0.5 M HCl) and (2) the crystalline Fe that is present as Fe(III) (oxyhydr)oxides (via CBD). These complement total Fe(II) and Fe(III) data reported in Krone *et al.* (2021b). Higher amounts (>7.6 mgFe g⁻¹ rock) of bioavailable Fe are associated with unaltered zones (Fig. 1a), while altered zones positively correlate with the presence of crystalline Fe

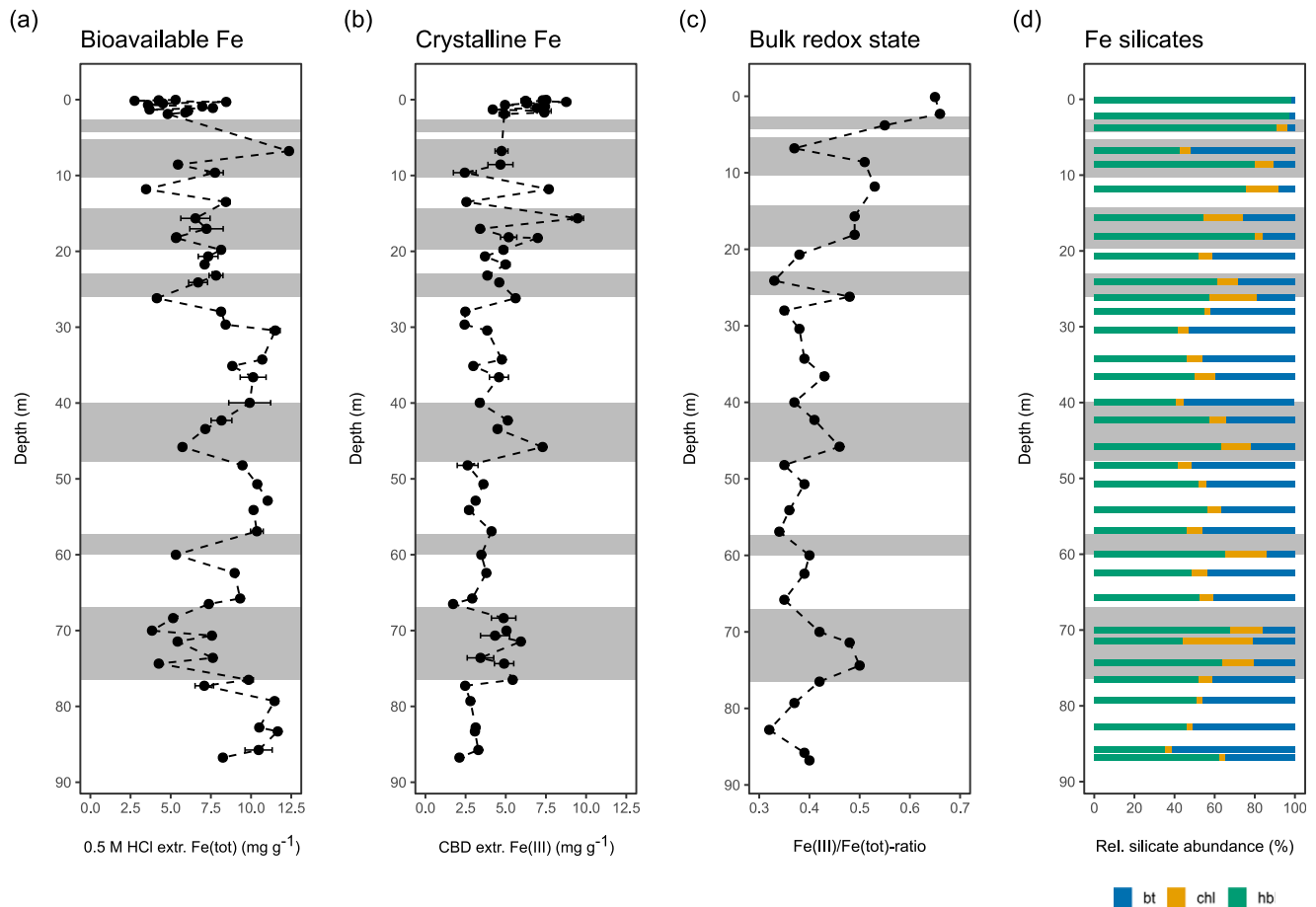


Figure 1. Geochemical, mineralogical and geophysical data of the Santa Gracia drill core. (a) 0.5 M HCl extractable Fe(tot) represents the bioavailable Fe pool, while (b) citrate-bicarbonate-dithionite (CBD) extractable Fe(III) is indicative of the amount of Fe(III) (oxyhydr)oxides (crystalline Fe) present. Data points in (a) and (b) represent the average of technical extraction replicates. Error bars denote the standard error of the technical extraction replicates. (c) Redox state of bulk drill core samples displayed as Fe(III)/Fe(total) ratios (replotted after Krone *et al.*, 2021b; Hampl *et al.*, 2022). (d) Relative abundances of Fe-bearing silicates biotite (bt), chlorite (chl) and hornblende (hbl) (modified after Hampl *et al.*, 2022). Grey boxes display the presence of prominent reddish zones, fracture (zones) and zones of correlating mineral abundances (see Weckmann *et al.*, 2020). Hampl *et al.* (2022) provides a more detailed overview of the connections between fracture zones, hydrothermal alteration and mineral abundances (see Figs 2–4).

(2.5–9.5 mg Fe g⁻¹ rock) (Fig. 1b). The Fe(III) (oxyhydr)oxide depth profile (Fig. 1b) mirrors the pattern of the bulk Fe(III)/Fe(total)-ratio profile (Fig. 1c) (see Krone *et al.*, 2021b). The Fe extraction data also complement previous analysis of the bulk mineralogy of the core samples (Fig. 1d) (Hampl *et al.*, 2022). This highlights a zone of particularly intense weathering and hydrothermal alteration in the deepest weathering zone (67–77 m depth) rich in Fe(III).

Furthermore, high-resolution water-extractable organic carbon (DOC) and nitrate data were obtained for the whole SG weathering profile (Fig. S9). DOC and nitrate potentially serve as electron donors and acceptors for microbial Fe(III) reduction and Fe(II) oxidation, respectively. The amount of DOC in the deep (<2 m) subsurface (0.17 mg g⁻¹ rock) on average was lower compared to the uppermost soil horizon (0–2 m, 0.25 mg g⁻¹ soil), as it was for nitrate (<2 m vs 0–2 m, 0.0008 vs 0.0035 mg g⁻¹ rock). The mean pH of the SG weathering profile was 8.20 ± 0.02 (potential pH) and 9.31 ± 0.04 (active pH) (*N* = 10, technical extraction triplicates) (Fig. S10).

Gibbs free energy of metabolic reactions with Fe-bearing minerals

We calculated Gibbs free energy yields for 38 Fe redox reactions based on the previously reported primary Fe-bearing minerals

(Krone *et al.*, 2021b; Hampl *et al.*, 2022) and secondary minerals formed by weathering (Fig. 2, Tables 1, S4). Overall, there is a wide range from highly exergonic (i.e. release of energy) to highly endergonic (i.e. requires energy supply) yields depending on the electron donor and acceptor chosen. Of 14 Fe(II) oxidation reactions listed (Table 1), 10 reactions are exergonic when coupled to either oxygen or nitrate reduction (Fig. 2a,b). With regard to primary Fe(II)-bearing minerals, there is a clear energetic benefit for microbial Fe(II) oxidation in biotite and hornblende with either oxygen or nitrate as an electron acceptor. Magnetite and free Fe(II) in solution could also fuel microaerophilic and/or nitrate-dependent Fe(II) oxidation, while chlorite oxidation would not provide enough energy to be energetically feasible. Moreover, reactions with nitrate as an electron acceptor could provide more energy than oxygen, e.g. in the case of magnetite being the electron donor.

In stark contrast to the situation for microbial Fe(II) oxidation, microbial Fe(III) reduction always requires the availability of Fe(III) (oxyhydr)oxides as an electron acceptor (Fig. 2c–e), while assuming free Fe²⁺ to be the Fe(II) product (Table 1). Of 24 Fe(III) reduction reactions listed, only 12 reactions are exergonic when coupled to either dihydrogen, acetate or lactate. Reduction of Fe(III)-bearing silicates are all endergonic, meaning there is no energetic advantage

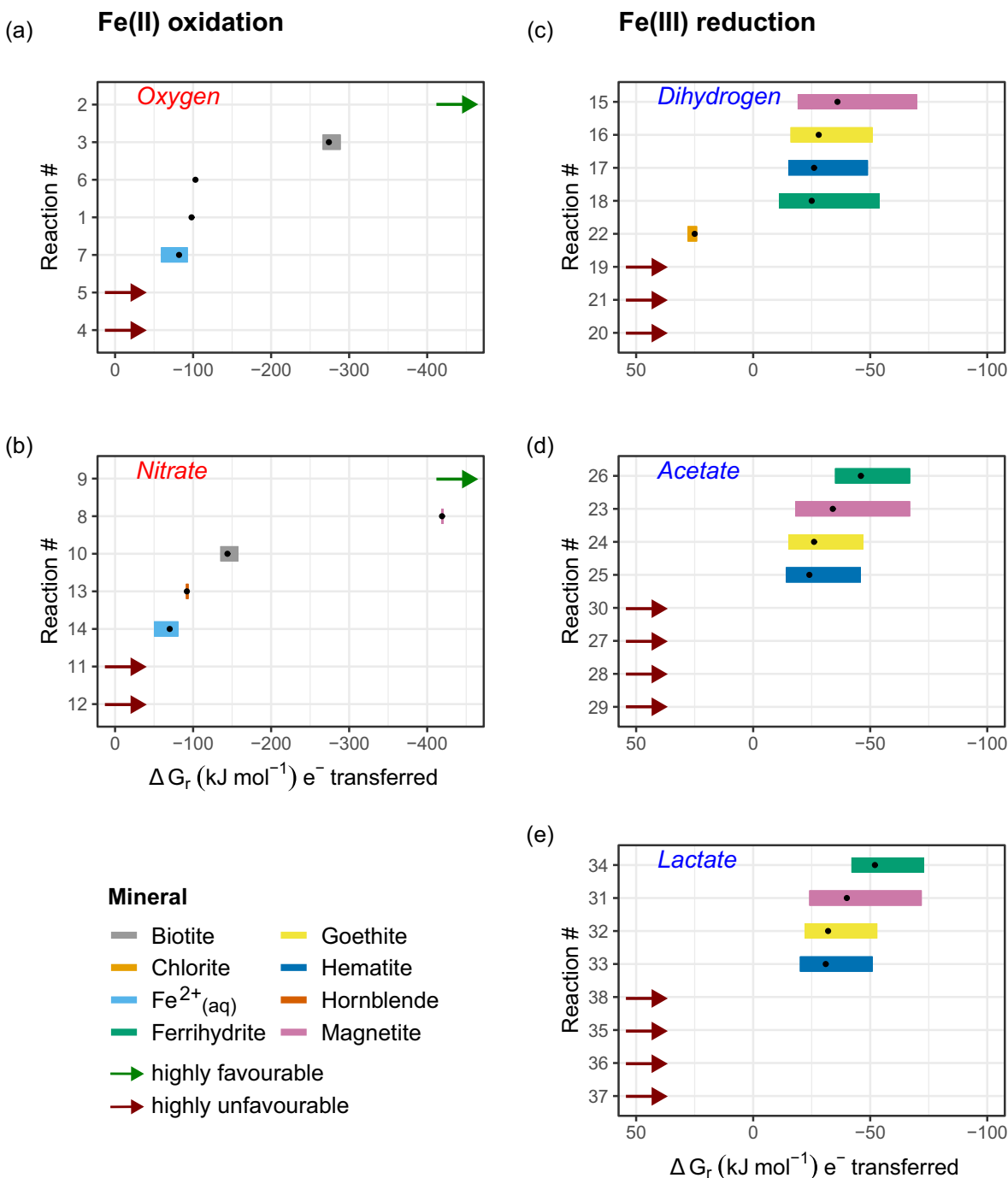


Figure 2. Gibbs free energy of Fe(II) oxidation and Fe(III) reduction redox reactions per electron transferred for *in situ* conditions. The 38 redox reactions (1–38) represent 14 oxidation (left column) and 24 reduction (right column) reactions for major Fe-bearing minerals present in the Santa Gracia (SG) depth profile (Table 1). Gibbs free energy per mole of electron transferred is shown for Fe(II) oxidation coupled to (a) O_2 reduction and (b) nitrate reduction (electron acceptors indicated in red letters), as well as for Fe(III) reduction coupled to (c) dihydrogen oxidation, (d) acetate oxidation and (e) lactate oxidation (electron donors indicated in blue letters). Gibbs free energy values of redox reactions are shown for fixed concentrations and a pH range of 6–9. Black dots represent Gibbs free energy values of redox reactions for pH 8, which is about the potential *in situ* pH of SG bulk drill core samples (Fig. S10). Gibbs free energy values of Fe(II) oxidation reactions 4, 5, 11 and 12 are not displayed because they are highly positive and hence not thermodynamically favourable, or in the case of reactions 2 and 9, unrealistically favourable (potentially due to the unreliable ΔG_r^0 database for Fe-bearing silicates). Energetic yields for reactions 1 and 8 (= magnetite) and 6 and 13 (= hornblende) show narrow to no ranges, as they are marginally to non-dependent from pH. Energetic yields for Fe(III) reduction reactions 19–21, 27–30 and 35–38 are not shown as they are highly unfavourable.

for microorganisms to use these minerals as an Fe(III) source. Reduction of Fe(III) (oxyhydr)oxides showed the strongest dependence on pH, specifically decreasing in energy yield with increasing pH but still being feasible up to pH 9.

Fe(III) reduction by *in situ* microbial communities

As Fe(III) (oxyhydr)oxides are abundant in fracture zones marked by weathering and/or hydrothermal alteration, and thermodynamic calculations demonstrated their potential as prevalent

Fe(III) sources, Fe(III) reduction enrichments were set up to identify depths in which the *in situ* community could be activated to perform Fe(III) reduction. Microbial Fe(III) reduction could be observed in screening/enrichment setups with ground rock powder (amended with ferrihydrite) throughout the whole weathering profile (Fig. 3), independent of the provided electron donor. In contrast, enrichments of Fe(II) oxidisers were successful for eight depths.

To determine whether altered zones act as hot spots for Fe(III)-reducing microbial activity, we investigated the effect of alteration on the concentrations of bioavailable Fe, crystalline Fe and Fe(III) reduction (Figs S6–S8). In the presence of alteration, we found a significant decrease in bioavailable Fe by 2.1 mg g⁻¹ rock (+alt = -2.06, $t = -4.9$, $df = 92$, $P < 0.001$) and a significant increase in crystalline Fe by 1.4 mg g⁻¹ rock (+alt = 1.371, $t = 4.7$, $df = 92$, $P < 0.001$). However, once the effect of depth is considered, Fe(III) reduction in altered and unaltered zones does not appear to be substantially different (Fig. 3), which is supported by Fig. S8 showing no significant effect of alteration on Fe(III) reduction. Contrastingly, depth ($t = 5.0$, $df = 92$, $P < 0.001$) and increased bioavailable Fe concentrations ($t = 5.1$, $df = 92$, $P < 0.001$) did both

significantly increase the amount of Fe(III) reduction (Figs S11, S12), unlike crystalline Fe (Fig. 13). It is noteworthy that the deepest unaltered zone sampled did have substantially greater Fe(III) reduction than the altered zone above it (H₂: 47.5 vs 28.6%; organics: 46.1 vs 37.3%) (Table S1).

To better understand Fe(III) reduction by *in situ* microbial communities along the SG weathering profile, we analysed the data using a LM. We used AIC model selection to distinguish among a set of possible statistical models describing the relationship between setup type (control ‘-Fhy’ vs experiment ‘+Fhy’), electron donor (H₂ vs organics), depth, bioavailable (poorly crystalline) Fe (Fe_{bio}), crystalline Fe (Fe_{cryst}) and Fe(III) reduction (Table S2). The best-fit model, carrying 94% of the cumulative model weight, included every parameter with three interaction effects (AIC = 907.2). It explains 50.4% of the variation in Fe(III) reduction (= adjusted R²) (Table S3) and has a significant fit to the data ($F = 15.59$, $df = 8$, 107, $P < 0.001$), leaving a residual standard error of 11.54 with 107 degrees of freedom. The LM identified the setup type, electron donor, depth, Fe_{bio} and the interaction depth:Fe_{bio} to be highly significant ($P < 0.001$), while the term Fe_{cryst} and the interactions setup:Fe_{bio} and depth:Fe_{cryst} were found to be significant ($P < 0.05$).

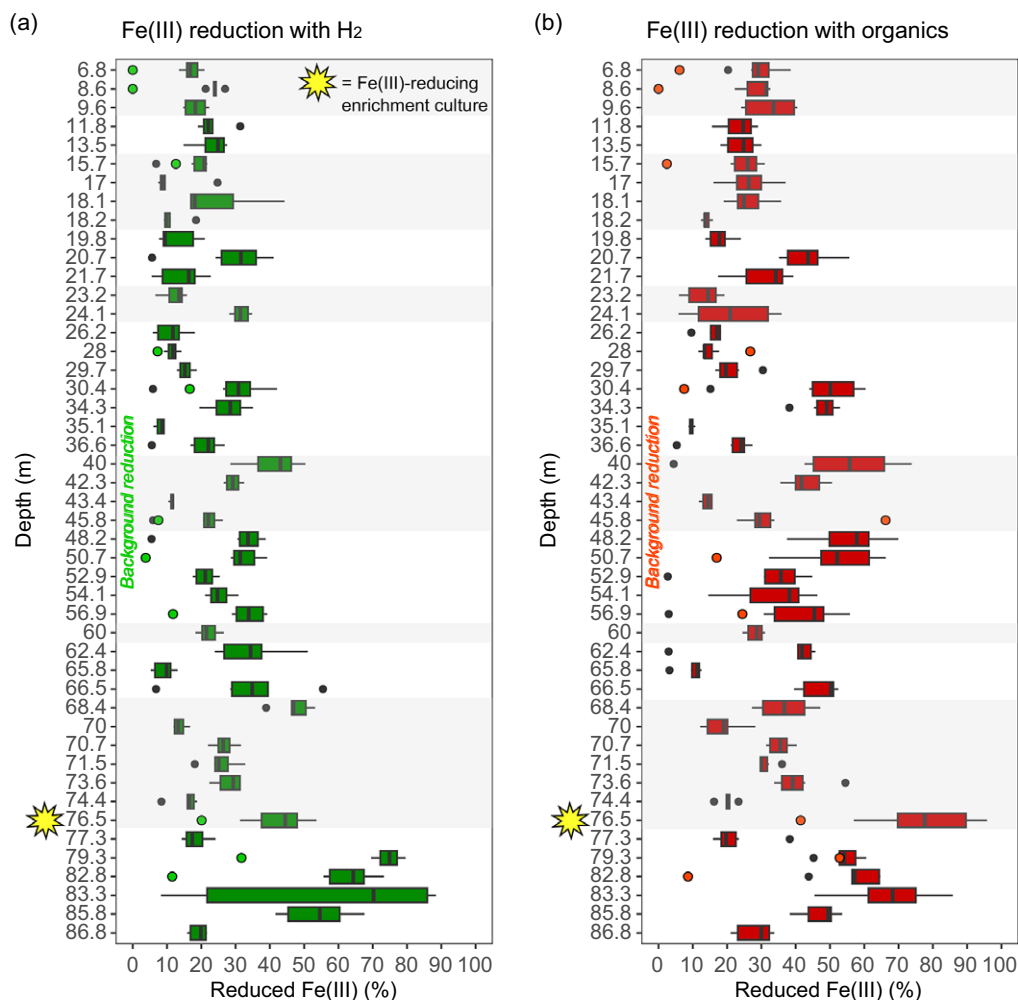


Figure 3. Fe(III) reduction by the *in situ* microbial community in the weathering profile of Santa Gracia. Drill core samples were amended with 5 mM ferrihydrite (Fhy) (= electron acceptor) and either (a) dihydrogen (H₂) in excess or (b) 5 mM acetate and lactate (= electron donor). Relative amount of microbially reduced Fe(III) in the experimental setups (= Fe from mineral powder with Fhy addition ‘+Fhy’; boxplots) is compared to Fe(III) reduction in the control setups (= Fe from mineral powder without Fhy addition ‘-Fhy’, identical to background reduction; filled, light-coloured circles). Fe concentrations were determined after 6–8 weeks of incubation. Boxplots show the variance of six biological replicates for each depth. Black dots represent boxplots outliers. Grey boxes display the presence of prominent reddish zones and fracture (zones).

Six *post hoc* paired-samples *t*-tests, corrected with Holm's sequential Bonferroni procedure (Table S4), indicated that the extent of Fe(III) reduction is (1) significantly larger in the experimental setups than in the control setups and (2) significantly larger in the organics setups than in the H₂ setups (Figs S14, S15). The mean Fe(III) reduction extent between the two electron donor treatments differed by 6.8% (H₂ vs organics: 32.8 to 26.0%).

Fe(II) oxidation by *in situ* microbial communities

Enrichments of Fe(II) oxidisers were successful for eight out of 47 samples (~17%) from 30.4, 34.3, 35.1, 40.0, 43.3, 50.7, 70.7 and 73.6 m depth. We identified growth in FeS tubes by the formation of distinct orange Fe(III) mineral accumulations within or below the orange-coloured top layer. Subsequent cultivation and isolation attempts were not successful.

Ferrihydrite microcosms with enrichment culture SG from the deep subsurface

Growth of Fe(III)-reducing enrichment culture. While microbial Fe(III) reduction could be observed in screening (i.e. positive enrichment) setups with ground rock powder throughout the whole weathering profile, a robust Fe(III)-reducing enrichment culture could only be obtained from crushed rock sample of a single depth interval located within the deepest identified weathering zone at ~77 m depth. The obligately anaerobic culture can grow chemoheterotrophically with lactate as well as autotrophically with dihydrogen as an electron donor but cannot oxidise acetate. Prior to its usage in batch ferrihydrite reduction experiments, the culture was pre-grown on 30 mM bicarbonate-buffered anoxic mineral medium (see Supporting Information methods for medium composition) and had been transferred six times. The dominant sequence (relative abundance of ~98.5%) in the enrichment culture community composition analysis was found to be 100% identical to the spore-forming sulfate-reducing *Desulfotomaculum ruminis* (Coleman, 1960; Spring *et al.*, 2012). It is noteworthy that the crushed rock powder sample contains about 9 μM MQ-water extractable sulfate per gram of powder while 2 mM sodium sulfate is included in the growth medium.

Batch ferrihydrite reduction experiments were conducted to determine which electron donors are used by the enrichment culture to reduce Fe(III). Ferrihydrite reduction was observed in setups with the addition of acetate/lactate, lactate and dihydrogen, but not in setups with acetate addition alone (Figs 4, S16). Generally, 4–5 mM added Fe(III) was completely reduced within 11–14 days in both acetate/lactate and dihydrogen setups. The main difference between these was the lag phase observed in the acetate/lactate setup (11 days), which was not observed in the dihydrogen setup (Fig. 4). Additionally, we observed that the Fe(II) concentration in solution rose during ferrihydrite reduction but quickly decreased again once the major part of Fe(III) (~85%) had been reduced. This might be due to interaction of dissolved Fe(II) with reduced sulfur species. As this strain is closely related to a known sulfate-reducing microorganism and there is some sulfate present in the growth medium, we also measured sulfate concentrations during the incubations, which decreased from ~1.8 to 0 mM (Fig. S16). Together these observations suggest a complex interplay of processes is occurring in the batch reactors driven by (1) Fe(III) reduction by Fe(III)-reducing microorganisms, (2) sulfate reduction by sulfate-reducing microorganisms and (3) further reaction between the products of these two processes (Fe(II) and sulfide) in the solution.

Microbial community sequencing

In situ and enrichment culture samples were independently sequenced and analysed. 16S-rRNA sequencing was conducted based on total DNA extracted from the uncontaminated inner rock core as well as from the final timepoint of Fhy microcosms for comparison (Fig. 5). Figure 5 shows enrichment culture community compositions of ferrihydrite microcosms amended with substrates with which culture SG can grow, i.e. dihydrogen ('+H₂') or lactate ('+Lactate'). Overall, *in situ* and enrichment culture compositions clearly differ, although it should be highlighted that separate sequencing and analysis for each composition could lead to batch effects. The *in situ* community composition displays a variety of ASVs typical for extreme environments. Only the two low abundant ASVs (genus level) *Sideroxydans* (0.04%) and *CL500_29_marine_group* (0.15%) can be attributed to the Fe cycle, here in the form of microaerophilic

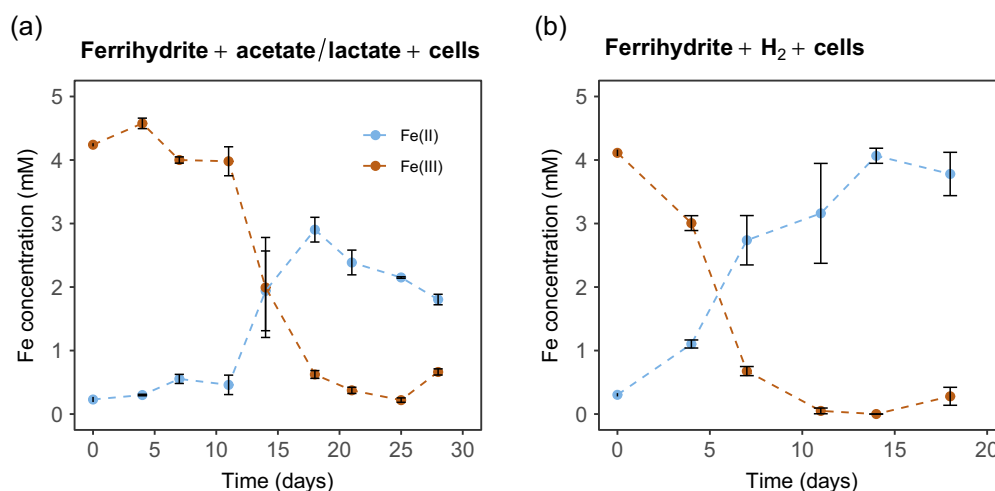


Figure 4. Ferrihydrite reduction by the enrichment culture obtained from the deepest weathering zone (~77 m depth) of the Santa Gracia weathering profile. An Fe(III)-reducing enrichment culture (culture SG) obtained from this zone was inoculated into microcosms (6th transfer, 10% (v/v)) to identify the preferential substrate condition. Microcosms were set up with 5 mM ferrihydrite (Fhy) (= electron acceptor) and either (a) 5 mM acetate and lactate or (b) dihydrogen (H₂) in excess (= electron donor). Further treatments with acetate or lactate addition as sole electron donor as well as control setups can be found in the Supplementary Material (Fig. S16). Microbially driven Fe(III) reduction is shown over time. Data points in (a) and (b) represent the average of three biological replicates. Error bars denote the standard error of the biological replicates.

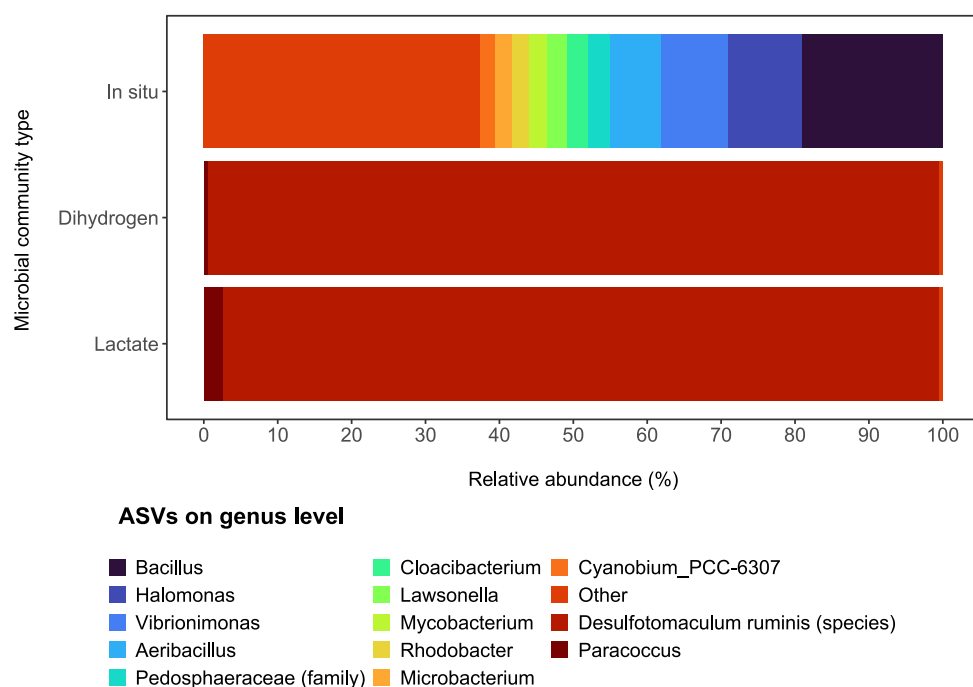


Figure 5. Comparison of *in situ* (= native) community composition versus enrichment culture community composition retrieved from identical drill core samples from ~77 m depth. *In situ* and enrichment culture samples were independently sequenced and analysed. The *in situ* community composition (“*In situ*”) reflects the relative amplicon sequence variants (ASV) abundance pre-enrichment (top panel). Enrichment culture compositions reflect shifted community compositions after substrate addition of ferrihydrite and dihydrogen (H₂) (“*Dihydrogen*”) or ferrihydrite and lactate (“*Lactate*”) (shown ASVs represent average abundances of three biological replicates; mid and bottom panel). In the top panel (“*In situ*”), relative abundances of the 15 most abundant ASVs (“*top15*”) are shown. The remaining genera ≤2.0% are summarised in “*Other*”. In the middle (“*Dihydrogen*”) and bottom (“*Lactate*”) panels, only two ASVs with a cumulative abundance of 99.5% are displayed. Genera <0.2% are summarised in “*Other*”.

Fe(II)-oxidising microorganisms. The two enrichment culture communities are dominated by a single ASV (species level) related to *Desulfotomaculum ruminis*, a sulfate-reducing strain.

Discussion

Potential for Fe-cycling in the deep biosphere of a semi-arid region

Localisation of relevant depth intervals for microbial weathering of Fe-bearing minerals. The SG weathering profile comprises multiple weathering zones that are partly situated in Fe-rich hydrothermally overprinted intervals of the profile (Krone *et al.*, 2021b; Hampl *et al.*, 2022). However, it is unknown if these locations represent hotspots for microbial activity and if microbial metabolisms contribute to subsurface weathering processes at the study site. We found that unaltered zones are locations of enhanced Fe bioavailability with poorly crystalline Fe serving as potential electron acceptor for microbial Fe metabolisms. In contrast, hydrothermally overprinted fractures and fracture zones were found to be composed of more crystalline Fe(III) (oxyhydr)oxides, which hampers microbial Fe(III) reduction. However, a particularly intense hydrothermal alteration in the deepest identified weathering zone (67–77 m depth) hosts a microbial community that is probably contributing to weathering processes at depth (Fig. 1). The presence of highly abundant bioavailable Fe(II) (Fig. 1a) indicates the potential of this environment to act as a habitat for Fe(II)-oxidising microbes, which is supported by the positive results of microaerophilic Fe(II)-oxidising enrichment cultures from numerous rock samples taken throughout the depth profile.

To facilitate microbial Fe(II) oxidation/Fe(III) reduction, Fe species also need to be accessible (Figs. 2, 3). Abiotic processes like weathering-induced fracturing make mineral surfaces more accessible for microbial Fe(II) oxidation, but also consume O₂ (Isherwood and Street, 1976; Kim *et al.*, 2017). Despite this enhanced mineral surface accessibility, it could be argued that microbial Fe(II) oxidation

is outcompeted by abiotic Fe(II) oxidation at an *in situ* pH ~8 (Fig. S1) (see Peiffer *et al.*, 2024). However, the measured pH of ground bulk core samples might be biased towards higher values by carbonates such as calcite, which were identified in hydrothermally altered fractures and fracture zones (Fig. S17) (see Krone *et al.*, 2021b; Hampl *et al.*, 2022). Our results suggest that there is potential for both Fe(II) oxidation and Fe(III) reduction (Figs 1, 2, S1, S2). While microbial Fe(II) oxidation is relevant in parts of the weathering profile, microbial Fe(III) reduction was identified over the entire depth profile (Fig 3).

Thermodynamic constraints on microbial weathering of Fe-bearing minerals. To study the potential impact of Fe-metabolising microbes on the weathering of primary and secondary Fe-bearing minerals within the SG weathering profile, energetically favourable Fe redox reactions were identified. Gibbs free energy yields for microbial Fe(II) oxidation were found to be favourable if the Fe source was magnetite or free Fe(II) in solution, and, to a lesser extent, biotite and hornblende (Fig. 2). However, because Fe(II) is strongly bound in the crystal structure of poorly soluble, highly crystalline biotite and hornblende, it is less accessible for microbial redox reactions (Shelobolina *et al.*, 2012; Napieralski *et al.*, 2019; Fan *et al.*, 2023). Fe(II) oxidation in pure biotite has been demonstrated previously, but only under laboratory conditions using very fine-grained (<5 μm) biotite (stock suspension concentration of 15–20 g l⁻¹) (Shelobolina *et al.*, 2012). These conditions and characteristics do not match the natural samples we were analysing. Thermodynamic calculations and the incorporation of Fe as structural Fe(II) in Fe(II)-bearing silicates suggest that primary Fe(II) minerals are probably not suitable as a main Fe source for Fe(II) oxidisers at our study site. Nonetheless, initial cultivation success of Fe(II)-oxidising microorganisms demonstrates their *in situ* existence, while not providing information on how active they are in *in situ* weathering of Fe(II)-bearing minerals. Hence, we can conclude that Fe-metabolising microorganisms are likely not the main driving force for weathering of primary Fe(II)-bearing silicates. In contrast, Fe(III) reduction is energetically feasible for microbes with magnetite and Fe(III) (oxyhydr)oxides like hematite,

goethite or ferrihydrite (Crosby *et al.*, 1983). Based on our calculation results and building on the minerals identified in the rock samples, we conclude that the deep biosphere at our study site is preferentially using secondary Fe(III) (oxyhydr)oxides for their metabolism.

Importance of the semi-arid climatic setting on microbial weathering

The semi-arid nature of the climatic setting at our field site SG is of importance when evaluating the potential for microbial Fe-cycling in the deep subsurface. Unlike for weathering profiles situated in more humid climates, the supply of meteoric water into the subsurface of SG via fractures and hence the transport of O₂, CO₂ and nutrients essential for microbial Fe redox reactions are limited (Napieralski *et al.*, 2019; 2022). Furthermore, organoheterotrophic-based subsurface microbial activity in (semi-)arid climates heavily feeds on the input of young organic C (Scheibe *et al.*, 2023). These limitations in available amounts of water and nutrients force Fe-metabolising microorganisms towards most energy-efficient redox reactions to ensure survival (Figs 2, S1, S2). Alternatively, microorganisms can form endospores or minimise their genome size (to reduce the cost of replication) to facilitate survival under water and nutrient deprivation (Lin *et al.*, 2006; Chivian *et al.*, 2008; Suzuki *et al.*, 2017; Fones *et al.*, 2019). In short, microbial weathering activity in our semi-arid deep weathering profile will only occur where environmental conditions allow for Fe redox reactions.

Fe-metabolising microorganisms are weathering agents

In our *in situ* Fe(III) reduction enrichments, we demonstrated that microbial Fe(III) reduction occurs with both H₂ and organics as electron donor (Figs 3, S14, S15). Overall, on average 6.8% more Fe(III) was reduced in the '+Fhy' setups with organic carbon added compared to setups with dihydrogen. This has two plausible explanations. First, bicarbonate was the only previously identified C source in the dihydrogen setups and thus the differences in Fe reduction extent may be related to different efficiencies of autotrophic vs heterotrophic carbon metabolism. Secondly, the observation might be a result of the higher energetic yield of Fe(III) reduction coupled to acetate/lactate oxidation over dihydrogen oxidation (see energy densities of reactions #18, 26 and 34; Fig. S1). Fe(III) reduction extent in unaltered versus altered zones in the setup with organics added (Fig. 3b) does not seem to be strongly influenced by the *in situ* DOC concentrations (Fig. S9). Organic carbon is most probably transported from the surface via the fracture network (Krumholz *et al.*, 1997). Zones of hydrothermal alteration did not show significantly more Fe(III) reduction (Fig. S8), thus partially ruling out our initial hypothesis that hydrothermally altered zones function as hot spots for Fe(III)-reducing microbial activity.

Regarding microbial Fe(II) oxidation, the failure to subsequently cultivate microaerophilic Fe(II)-oxidising microorganisms does not invalidate the fact that they grew initially. As abiotic Fe(II) oxidation can be ruled out based on the conducted control experiments, observed growth suggests that gradient tubes were an accurate measure of microbial Fe(II)-oxidising activity. In summary, these results suggest that microbial Fe(III) reduction is relatively more important than microbial Fe(II) oxidation with regard to transformation of Fe-bearing minerals in the subsurface.

Evidence for microbial weathering of Fe-bearing minerals from community sequencing

We were able to enrich a robust Fe(III)-reducing culture (Fig. 4) and we can rule out that the obtained enrichment culture has entered the subsurface via a contamination, a common risk when retrieving

subsurface samples. This leads us to be confident that the detected taxon *Desulfotomaculum* in the enrichment culture (abundance of 98.5%) is part of the *in situ* community (Fig. 5), even though it is not abundant (<0.01%) in the detected *in situ* ASVs. The taxon has also been found in other subsurface environments, including uranium/heavy metal-contaminated aquifers, freshwater and marine sediments, mines and oil reservoirs (Magot *et al.*, 2000; Chang *et al.*, 2001; Kaksonen *et al.*, 2006; Ollivier *et al.*, 2007; Wang *et al.*, 2008; Aullo *et al.*, 2013).

Desulfotomaculum ruminis is capable of Fe(III) and sulfate reduction (Figs 4, S16), while it is unclear if Fe(III) reduction was driven directly (i.e. direct Fe(III) reduction) or indirectly by the oxidation of sulfide produced by this culture. Given that culture SG is able to reduce Fe(III) and sulfate, genera related to Fe(III) and sulfate reduction, as well as Fe(II) and sulfur oxidation are expected. Genera and species confirming this assumption are *Thiomonas*, *Pseudomonas kujiense*, *Chlorobium*, *Thiodictyon*, *Rhodoferrax*, *Flavobacterium*, *Paludibacter blasticus*, *Gallionella capsiferiformans*, *Sulfuricurvum kujiense* and *Thiodictyon ruminis* (Widdel *et al.*, 1993; Ehrenreich and Widdel, 1994; Heising *et al.*, 1999; Finneran *et al.*, 2003; Croal *et al.*, 2004; Harris *et al.*, 2004; Kodama and Watanabe, 2004; Hegler *et al.*, 2008; Gregersen *et al.*, 2009; Hegler *et al.*, 2010; Zhuang *et al.*, 2011; Walter *et al.*, 2014; Fabisch *et al.*, 2016; Gauger *et al.*, 2016; Ghosh *et al.*, 2018; Akob *et al.*, 2020; Ross *et al.*, 2022). They could also be quantified in minor (<0.01%) to larger (up to 8.5%) amounts in the enrichments in this study (Fig. 5). In summary, this suggests a potential interconnection between microbial Fe and S cycles in the culture (Fig. 6; Supporting Information Discussion section). There is the possibility of microbial sulfate reduction-driven weathering of Fe-bearing minerals, but the low amount of quantified S in the rock suggests the impact of S *in situ* is limited.

The *in situ* community composition in the deepest weathering zone is not dominated by ASVs related to microbial Fe(III) and sulfate reduction. Most abundant ASVs are related to microorganisms living in the rhizosphere (*Bacillus* [12.5%]), saline (*Halomonas* [10.1%]) or hot environments (*Aeribacillus* [4.6%], *Mycobacterium* [2.4%] and *Rhodobacter* [2.3%]), metabolizing complex hydrocarbon compounds (*Lawsonella* [2.8%] and *Vibrionimonas* [9.1%]) or fixing N₂ (*Pedospaeraceae* [3.0%]) (Fig. 5) (see Schröder *et al.*, 1997; Cruz-Martínez *et al.*, 2009; Yasawong *et al.*, 2011; Filippidou *et al.*, 2015; Khan *et al.*, 2019; Xian *et al.*, 2020; Campbell *et al.*, 2021; Mahmoud *et al.*, 2023). Moreover, *in situ* ASVs of minor relative abundance (≤2%) can be assigned to genera related to microorganisms oxidising Fe(II), sulfur and H₂ (*Sideroxydans* [<0.01%]) and utilising carbohydrates (*CL500_29_marine_group* [0.2%]) (see Warnecke *et al.*, 2004; Lüdecke *et al.*, 2010; Liu *et al.*, 2015; McIlroy *et al.*, 2017; Chen *et al.*, 2020; Cooper *et al.*, 2023). Natural abiotic H₂ gas can originate from biotite hydration in granite (Murray *et al.*, 2020) or rock comminution (i.e. fracture-induced water reduction) (Sato *et al.*, 1984; Klein *et al.*, 2020). Overall, the sequencing results of the *in situ* community might be explained by the low cell abundance of specific strains and high degree of adaptation and specialisation in such a water- and nutrient-deprived subsurface system. In summary, the ASVs identified from the deep subsurface of our study site paired with the geochemical/mineralogical setting most probably indicate microbial involvement in (1) Fe(II), sulfur and H₂ oxidation, (2) Fe(III) and sulfate reduction, and (3) complex hydrocarbon compound metabolism. To account for the possibility of cryptic sulfur cycling in this context, we considered the stoichiometry of probable Fe-S redox reactions (Supplementary Material Discussion section).

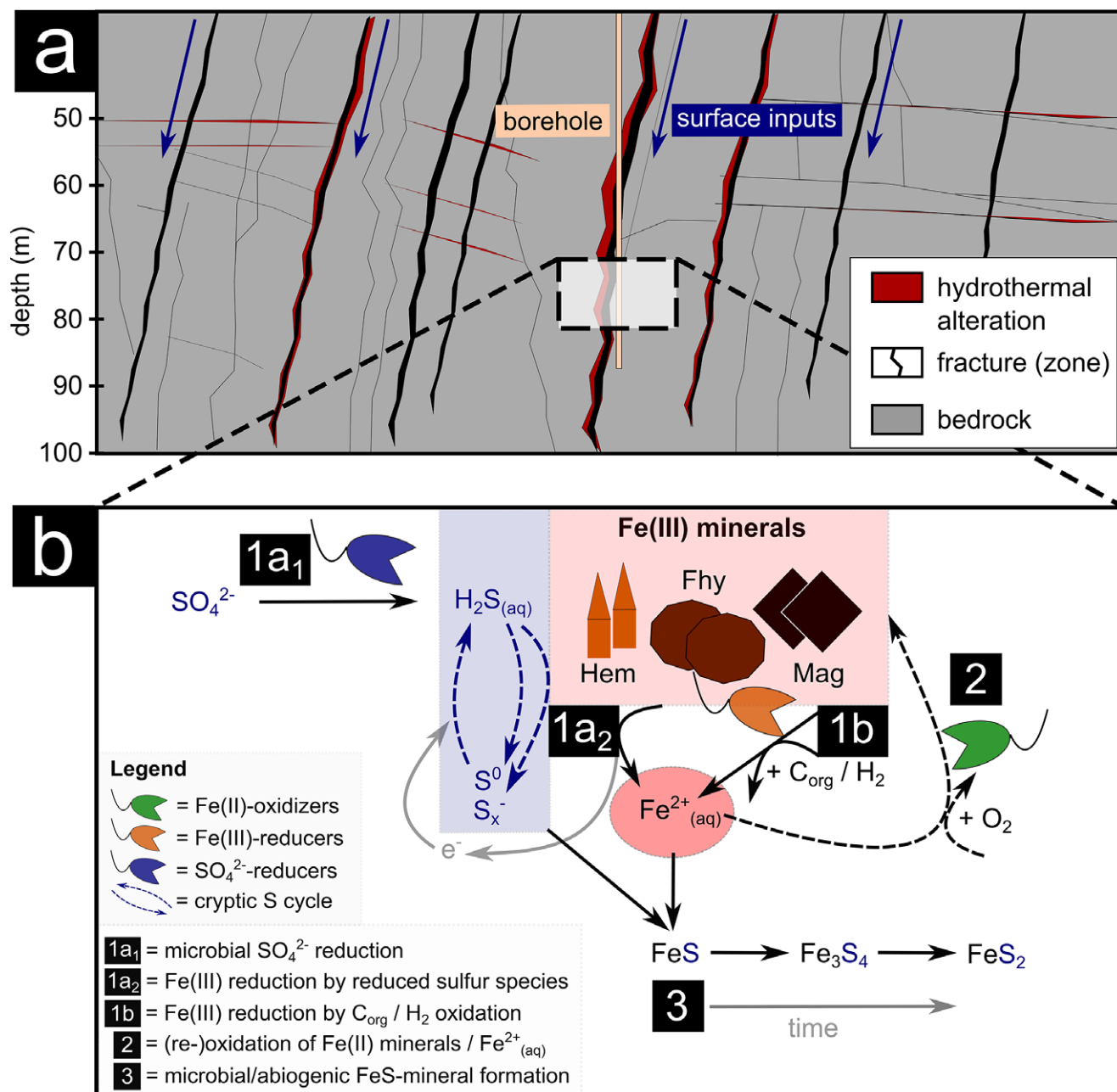


Figure 6. Summary of potential, microbially driven weathering scenario in the deepest weathering zone of the Santa Gracia (SG) weathering profile. (a) The subsurface is characterised by (tectonic) fracturing, hydrothermal alteration and weathering. Hydrothermal alteration and weathering are often superimposed. (b) Cartoon of a proposed microbially driven Fe cycle, interlinked with a S cycle in the deepest, hydrothermally altered SG weathering zone (~77 m depth, cf. Fig. 1). Sulfate-reducing microorganisms reduce sulfate with help of a non-organic energy source as Fe(III) to reduced sulfur species (step 1a₁). Subsequently, Fe(III) minerals can be reduced to Fe(II) when (a) reacting with highly reactive sulfur species (e.g. H_2S) (step 1a₂) or (b) coupled to oxidation of organic carbon or dihydrogen (H_2) (step 1b). Formed Fe(II) species are reoxidised by Fe(II)-oxidising microorganisms (step 2) and/or react with reduced sulfur species and form FeS minerals such as mackinawite or Fe(III)-mackinawite (step 3, Fig. S18). Over time, FeS minerals become more crystalline (Fe_3S_4 , FeS_2 formation). Reduced sulfur species can be reoxidised, fueling a cryptic S cycle and by that further amplifying Fe(III) reduction. The cryptic sulfur cycle component is probably more important in the enrichment culture than *in situ*. Abbreviations: SO_4^{2-} = sulfate; H_2S = dihydrogen sulfide; S^0 = elemental sulfur; S_x^- = other intermediate sulfur species; Hem = hematite; Fhy = ferrihydrite; Mag = magnetite; $\text{Fe}^{2+}_{(\text{aq})}$ = aqueous iron; FeS = (Fe(III)-)mackinawite; Fe_3S_4 = greigite; FeS_2 = pyrite; C_{org} = organic carbon; H_2 = dihydrogen; O_2 = oxygen.

Conclusions and environmental implications

This study has revealed the potential of microorganisms in weathering of Fe-bearing minerals in the deep subsurface of a semi-arid environment. We underpin its existence with a comprehensive cultivation approach of Fe(II)-oxidising and Fe(III)-reducing microorganisms under quasi-environmental conditions (growth conditions as close to the environment as possible).

To comprehensively consider the potential for microbial Fe cycling, we included all Fe-bearing minerals in our approach, including Fe-bearing silicates.

Our main conclusions are as follows.

- 1) Zones of unaltered and altered rock with increased concentration of bioavailable Fe provide an Fe pool that is accessible to microorganisms.

- 2) Fe present in fractured and hydrothermally altered zones are not hot spots for microbial Fe(III)-reducing activity because the minerals are probably less accessible due to their more crystalline nature.
- 3) Microorganisms are probably not contributing to the weathering of Fe(II)-bearing silicate minerals. Secondary Fe(III) (oxyhydr)oxides are required for microbial Fe(III) reduction and hence microbial weathering activity.
- 4) Fe and S cycles are potentially interconnected in the deepest, hydrothermally altered weathering zone of the SG weathering profile.
- 5) The microbiome of deep weathering zones has adapted towards the most energy-efficient redox reactions (organoheterotrophy and chemolithotrophy) to ensure survival in a water- and nutrient-deprived system.
- 6) In the deep subsurface, Fe-metabolising microorganisms contribute to weathering in both unfractured and fractured altered rock and need to be considered when investigating deep subsurface weathering processes, even within semi-arid environments.

Supplementary material. The supplementary material for this article can be found at <http://doi.org/10.1180/gbi.2025.2>.

Sample availability. The metadata of all the IGSN-registered samples used for this study (samples in Supplementary Information tables) can be accessed via [https://doi.org/10.60510/\(IGSN of sample\)](https://doi.org/10.60510/(IGSN of sample)).

Data availability. Additional supplementary tables (S1–S12, ST1–ST5), including raw data and thermodynamic calculations are available in the data publication Schwerdhelm *et al.* (2024), <https://doi.org/10.5880/figeo.2024.027>. The data publication is hosted by the GFZ data services. The raw sequencing data have been deposited at the Sequence Read Archive under BioProject accession number PRJNA1072308 (<https://www.ncbi.nlm.nih.gov/bioproject/PRJNA1072308>).

Author contribution. Christopher Schwerdhelm: conceptualization, methodology, investigation, writing – original draft preparation, writing – review & editing. Ferdinand J. Hampl: investigation, writing – review & editing. Laura V. Krone: investigation, writing – review & editing. Lea Sauter: investigation, writing – review & editing. Kari Kaphegyi: investigation, writing – review & editing. Lucas Horstmann: investigation, writing – review & editing. Daniel Straub: investigation, writing – review & editing. Toby S. Samuels: supervision, methodology, writing – review & editing. Muammar Mansor: supervision, methodology, writing – review & editing. Carolina Merino: writing – review & editing. Francisco Matus: writing – review & editing. Friedhelm von Blanckenburg: writing – review & editing. Dirk Wagner: writing – review & editing. Thomas Neumann: funding acquisition, writing – review & editing. Andreas Kappler: funding acquisition, supervision, writing – review & editing. Casey Bryce: funding acquisition, conceptualization, supervision, writing – review & editing.

Acknowledgements. This study was funded by the German science foundation (DFG) priority research program EarthShape: “Earth Surface Shaping by Biota” (grant no. BR 5927/2-1; KA 1736/54-1) and the EarthShape Coordination (EH 329/17-2, BL562/20-1). We are grateful to Dixie Rivera, Kirstin Übernickel, Lars Ganzert, Axel Kitte and Rómulo Oses for their support during the drilling campaign. We also thank the national park service of Chile (CONAF) for access to the study areas during field excursions. We further thank Monika Hertel and Björn Spranglewski for their help with IC measurements, Hanna Grimm for her help with DOC measurements, Verena Nikeleit for her help with HPLC measurements and culture maintenance/transfer, Franziska Schädler for her help with molecular microbiology sample preparation, Natalia Jakus for her help with μ XRD measurements, and Eric Runge for his help with Raman spectroscopy measurements.

Competing interests. None of the authors has any competing interests.

References

- Akob D.M. *et al.* (2020) Mixotrophic Iron-Oxidizing *Thiomonas* Isolates from an Acid Mine Drainage-Affected Creek. *Applied and Environmental Microbiology*, **86**(24), e01424–01420, <https://doi.org/10.1128/AEM.01424-20>.
- Aullo T., Ranchou-Peyruse A., Ollivier B. and Magot M. (2013) *Desulfotomaculum* spp. and related gram-positive sulfate-reducing bacteria in deep subsurface environments. *Frontiers in Microbiology*, **4**, <https://doi.org/10.3389/fmicb.2013.00362>.
- Bach W. and Edwards K.J. (2003) Iron and sulfide oxidation within the basaltic ocean crust: implications for chemolithoautotrophic microbial biomass production. *Geochimica et Cosmochimica Acta*, **67**(20), 3871–3887, [https://doi.org/10.1016/S0016-7037\(03\)00304-1](https://doi.org/10.1016/S0016-7037(03)00304-1).
- Banwart S.A., Nikolaidis N.P., Zhu Y.-G., Peacock C.L. and Sparks D.L. (2019) Soil functions: Connecting Earth’s Critical Zone. *Annual Review of Earth and Planetary Sciences*, **47**, 333–359.
- Barcellos D., O’Connell C., Silver W., Meile C. and Thompson A. (2018) Hot spots and hot moments of soil moisture explain fluctuations in iron and carbon cycling in a humid tropical forest soil. *Soil Systems*, **2**(4), 59.
- Barton K. and Barton M. (2015) Package ‘mumin’. Version, 1, 18. *R Foundation for Statistical Computing*, Vienna.
- Bazilevskaya E., Rother G., Mildner D.F., Pavich M., Cole D., Bhatt M.P., Jin L., Steefel C.I. and Brantley S.L. (2015) How oxidation and dissolution in diabase and granite control porosity during weathering. *Soil Science Society of America Journal*, **79**(1), 55–73.
- Bernhard N., Moskwa L.-M., Schmidt K., Oeser R.A., Aburto F., Bader M.Y., Baumann K., von Blanckenburg F., Boy J. and van den Brink L. (2018) Pedogenic and microbial interrelations to regional climate and local topography: new insights from a climate gradient (arid to humid) along the Coastal Cordillera of Chile. *Catena*, **170**, 335–355.
- Bochet O. *et al.* (2020) Iron-oxidizer hotspots formed by intermittent oxic–anoxic fluid mixing in fractured rocks. *Nature Geoscience*, **13**, 149–155, <https://doi.org/10.1038/s41561-019-0509-1>.
- Boettger J., Lin H.-T., Cowen J.P., Hentscher M. and Amend J.P. (2013) Energy yields from chemolithotrophic metabolisms in igneous basement of the Juan de Fuca ridge flank system. *Chemical Geology*, **337–338**, 11–19, <https://doi.org/10.1016/j.chemgeo.2012.10.053>.
- Bolyen E., Rideout J.R., Dillon M.R., Bokulich N.A., Abnet C.C., Al-Ghalith G. A., Alexander H., Alm E.J., Arumugam M. and Asnicar F. (2019) Reproducible, interactive, scalable and extensible microbiome data science using QIIME 2. *Nature Biotechnology*, **37**(8), 852–857.
- Brantley S.L., Goldhaber M.B. and Ragnarsdottir K.V. (2007) Crossing disciplines and scales to understand the critical zone. *Elements*, **3**(5), 307–314.
- Brantley S.L., Lebedeva M.I., Balashov V.N., Singha K., Sullivan P.L. and Stinchcomb G. (2017) Toward a conceptual model relating chemical reaction fronts to water flow paths in hills. *Geomorphology*, **277**, 100–117.
- Buss H., Bruns M., Schultz M., Moore J., Mathur C. and Brantley S. (2005) The coupling of biological iron cycling and mineral weathering during saprolite formation, Luquillo Mountains, Puerto Rico. *Geobiology*, **3**(4), 247–260.
- Buss H.L., Sak P.B., Webb S.M. and Brantley S.L. (2008) Weathering of the Rio Blanco quartz diorite, Luquillo Mountains, Puerto Rico: Coupling oxidation, dissolution, and fracturing. *Geochimica et Cosmochimica Acta*, **72**(18), 4488–4507.
- Caccavo F., Lonergan D.J., Lovley D.R., Davis M., Stolz J.F. and McInerney M.J. (1994) *Geobacter sulfurreducens* sp. nov., a hydrogen- and acetate-oxidizing dissimilatory metal-reducing microorganism. *Applied and Environmental Microbiology*, **60**(10), 3752–3759, <https://doi.org/10.1128/aem.60.10.3752-3759.1994>.
- Callahan B.J., McMurdie P.J., Rosen M.J., Han A.W., Johnson A.J.A. and Holmes S.P. (2016) DADA2: High-resolution sample inference from Illumina amplicon data. *Nature Methods*, **13**(7), 581–583.
- Campbell B.C., Gong S., Greenfield P., Midgley D.J., Paulsen I.T. and George S. C. (2021) Aromatic compound-degrading taxa in an anoxic coal seam microbiome from the Surat Basin, Australia. *FEMS Microbiology Ecology*, **97**(5), <https://doi.org/10.1093/femsec/fiab053>.
- Caporaso J.G., Lauber C.L., Walters W.A., Berg-Lyons D., Lozupone C.A., Turnbaugh P.J., Fierer N. and Knight R. (2011) Global patterns of 16S rRNA

- diversity at a depth of millions of sequences per sample. *Proceedings of the National Academy of Sciences*, **108**(supplement_1), 4516–4522.
- Cembrano J., González G., Arancibia G., Ahumada I., Olivares V. and Herrera V. (2005) Fault zone development and strain partitioning in an extensional strike-slip duplex: A case study from the Mesozoic Atacama fault system, Northern Chile. *Tectonophysics*, **400**(1), 105–125, <https://doi.org/10.1016/j.tecto.2005.02.012>.
- Chang Y.-J., Peacock A.D., Long P.E., Stephen J.R., McKinley J.P., Macnaughton S.J., Hussain A.K.M.A., Saxton A.M. and White D.C. (2001) Diversity and characterization of sulfate-reducing bacteria in groundwater at a uranium mill tailings site. *Applied and Environmental Microbiology*, **67**(7), 3149–3160, <https://doi.org/10.1128/AEM.67.7.3149-3160.2001>.
- Chen Y., Shao Z., Kong Z., Gu L., Fang J. and Chai H. (2020) Study of pyrite based autotrophic denitrification system for low-carbon source stormwater treatment. *Journal of Water Process Engineering*, **37**, 101414, <https://doi.org/10.1016/j.jwpe.2020.101414>.
- Chivian D. et al. (2008) Environmental genomics reveals a single-species ecosystem deep within Earth. *Science*, **322**(5899), 275–278, <https://doi.org/10.1126/science.1155495>.
- Coleman G. (1960) A sulphate-reducing bacterium from the sheep rumen. *Microbiology*, **22**(2), 423–436.
- Cooper R.E., Finck J., Chan C. and Küsel K. (2023) Mixotrophy broadens the ecological niche range of the iron oxidizer *Sideroxydans* sp. CL21 isolated from an iron-rich peatland. *FEMS Microbiology Ecology*, **99**(2), <https://doi.org/10.1093/femsec/fiac156>.
- Croal L.R., Johnson C.M., Beard B.L. and Newman D.K. (2004) Iron isotope fractionation by Fe(II)-oxidizing photoautotrophic bacteria. *Geochimica et Cosmochimica Acta*, **68**(6), 1227–1242.
- Crosby S.A., Glasson D.R., Cuttler A.H., Butler I., Turner D.R., Whitfield M. and Millward G.E. (1983) Surface areas and porosities of iron(III)- and iron(II)-derived oxyhydroxides. *Environmental Science & Technology*, **17**(12), 709–713, <https://doi.org/10.1021/es00118a004>.
- Cruz-Martínez K., Suttle K.B., Brodie E.L., Power M.E., Andersen G.L. and Banfield J.F. (2009) Despite strong seasonal responses, soil microbial consortia are more resilient to long-term changes in rainfall than overlying grassland. *The ISME Journal*, **3**(6), 738–744, <https://doi.org/10.1038/ismej.2009.16>.
- Di Tommaso P., Chatzou M., Floden E.W., Barja P.P., Palumbo E. and Notredame C. (2017) Nextflow enables reproducible computational workflows. *Nature Biotechnology*, **35**(4), 316–319.
- Ehrenreich A. and Widdel F. (1994) Anaerobic oxidation of ferrous iron by purple bacteria, a new type of phototrophic metabolism. *Applied and Environmental Microbiology*, **60**(12), 4517–4526.
- Ehrlich H.L. (1998) Geomicrobiology: its significance for geology. *Earth-Science Reviews*, **45**(1–2), 45–60.
- Emerson D. and Floyd M.M. (2005) Enrichment and isolation of iron-oxidizing bacteria at neutral pH. Pp. 112–123 in: *Methods in Enzymology* (J. Abelson and M.I. Simon, editors). Academic Press, Pasadena.
- Ewels P.A., Peltzer A., Fillinger S., Patel H., Alneberg J., Wilm A., Garcia M.U., Di Tommaso P. and Nahnsen S. (2020) The nf-core framework for community-curated bioinformatics pipelines. *Nature Biotechnology*, **38**(3), 276–278.
- Fabisch M., Freyer G., Johnson C.A., Büchel G., Akob D.M., Neu T.R. and Küsel K. (2016) Dominance of 'Gallionella capsiferriformans' and heavy metal association with Gallionella-like stalks in metal-rich pH 6 mine water discharge. *Geobiology*, **14**(1), 68–90, <https://doi.org/10.1111/gbi.12162>.
- Fan Q., Wang L., Fu Y., Li Q., Liu Y., Wang Z. and Zhu H. (2023) Iron redox cycling in layered clay minerals and its impact on contaminant dynamics: A review. *Science of The Total Environment*, **855**, 159003, <https://doi.org/10.1016/j.scitotenv.2022.159003>.
- Filippidou S., Jaussi M., Junier T., Wunderlin T., Jeanneret N., Regenspurg S., Li P.-E., Lo C.-C., Johnson S. and McMurtry K. (2015) Genome sequence of *Aeribacillus pallidus* strain GS3372, an endospore-forming bacterium isolated in a deep geothermal reservoir. *Genome Announcements*, **3**(4), 10.1128/genomea.00981–00915.
- Finneran K.T., Johnsen C.V. and Lovley D.R. (2003) *Rhodferax ferrireducens* sp. nov., a psychrotolerant, facultatively anaerobic bacterium that oxidizes acetate with the reduction of Fe(III). *International Journal of Systematic and Evolutionary Microbiology*, **53**(3), 669–673, <https://doi.org/10.1099/ijs.0.02298-0>.
- Fones E.M., Colman D.R., Kraus E.A., Nothaft D.B., Poudel S., Rempfert K.R., Spear J.R., Templeton A.S. and Boyd E.S. (2019) Physiological adaptations to serpentinization in the Samail Ophiolite, Oman. *The ISME Journal*, **13**(7), 1750–1762.
- Fredrickson J.K. and Balkwill D.L. (2006) Geomicrobial processes and biodiversity in the deep terrestrial subsurface. *Geomicrobiology Journal*, **23**(6), 345–356, <https://doi.org/10.1080/01490450600875571>.
- Friese A., Kallmeyer J., Axel Kitte J., Montaña Martínez I., Bijaksana S., Wagner D., the ICDP Lake Chalco Drilling Science and the ICDP Towuti Drilling Science Team (2017) A simple and inexpensive technique for assessing contamination during drilling operations. *Limnology and Oceanography: Methods*, **15**(2), 200–211.
- Gauger T., Byrne J.M., Konhauser K.O., Obst M., Crowe S. and Kappler A. (2016) Influence of organics and silica on Fe(II) oxidation rates and cell-mineral aggregate formation by the green-sulfur Fe(II)-oxidizing bacterium *Chlorobium ferrooxidans* KoFox – Implications for Fe (II) oxidation in ancient oceans. *Earth and Planetary Science Letters*, **443**, 81–89.
- Ghosh D., Bhadury P. and Routh J. (2018) Coping with arsenic stress: Adaptations of arsenite-oxidizing bacterial membrane lipids to increasing arsenic levels. *MicrobiologyOpen*, **7**(5), e00594.
- Gregersen L.H., Habicht K.S., Peduzzi S., Tonolla M., Canfield D.E., Miller M., Cox R.P. and Frigaard N.-U. (2009) Dominance of a clonal green sulfur bacterial population in a stratified lake. *FEMS Microbiology Ecology*, **70**(1), 30–41, <https://doi.org/10.1111/j.1574-6941.2009.00737.x>.
- Gu X., Heaney P.J., Reis F.D.A.A. and Brantley S.L. (2020) Deep abiotic weathering of pyrite. *Science*, **370**(6515), eabb8092, <https://doi.org/10.1126/science.abb8092>.
- Hampl F.J., Schipperski F., Byrne J.M., Schwerdhelm C., Kappler A., Bryce C., von Blanckenburg F. and Neumann T. (2021) Mineralogical, geochemical and magnetic susceptibility data from a deep hydrothermally altered profile in a semi-arid region (Chilean Coastal Cordillera). GFZ Data Services. 10.5880/fidgeo.2021.037.
- Hampl F.J., Schipperski F., Byrne J.M., Schwerdhelm C., Kappler A., Bryce C., von Blanckenburg F. and Neumann T. (2022) The role of iron-bearing minerals for the deep weathering of a hydrothermally altered plutonic rock in semi-arid climate (Chilean Coastal Cordillera). *Chemical Geology*, **604**, 120922, <https://doi.org/10.1016/j.chemgeo.2022.120922>.
- Harris J.K., Kelley S.T. and Pace N.R. (2004) New perspective on uncultured bacterial phylogenetic division OP11. *Applied and Environmental Microbiology*, **70**(2), 845–849, <https://doi.org/10.1128/AEM.70.2.845-849.2004>.
- Hegler F., Posth N.R., Jiang J. and Kappler A. (2008) Physiology of phototrophic iron (II)-oxidizing bacteria: implications for modern and ancient environments. *FEMS Microbiology Ecology*, **66**(2), 250–260.
- Hegler F., Schmidt C., Schwarz H. and Kappler A. (2010) Does a low-pH microenvironment around phototrophic FeII-oxidizing bacteria prevent cell encrustation by FeIII minerals? *FEMS Microbiology Ecology*, **74**(3), 592–600.
- Heidari P., Li L., Jin L., Williams J.Z. and Brantley S.L. (2017) A reactive transport model for Marcellus shale weathering. *Geochimica et Cosmochimica Acta*, **217**, 421–440, <https://doi.org/10.1016/j.gca.2017.08.011>.
- Heising S., Richter L., Ludwig W. and Schink B. (1999) *Chlorobium ferrooxidans* sp. nov., a phototrophic green sulfur bacterium that oxidizes ferrous iron in coculture with a "Geospirillum" sp. strain. *Archives of Microbiology*, **172**(2), 116–124, <https://doi.org/10.1007/s002030050748>.
- Holbrook W.S., Marcon V., Bacon A.R., Brantley S.L., Carr B.J., Flinchum B.A., Richter D.D. and Riebe C.S. (2019) Links between physical and chemical weathering inferred from a 65-m-deep borehole through Earth's critical zone. *Scientific Reports*, **9**(1), 4495, <https://doi.org/10.1038/s41598-019-40819-9>.
- Holm S. (1979) A simple sequentially rejective multiple test procedure. *Scandinavian Journal of Statistics*, **6**(2), 65–70.
- Isherwood D. and Street A. (1976) Biotite-induced grussification of the Boulder Creek Granodiorite, Boulder County, Colorado. *GSA Bulletin*, **87**(3), 366–370.
- Jones R.M., Goordial J.M. and Orcutt B.N. (2018) Low energy subsurface environments as extraterrestrial analogs. *Frontiers in Microbiology*, **9**(1605), <https://doi.org/10.3389/fmicb.2018.01605>.
- Kaksonen A.H., Spring S., Schumann P., Kroppenstedt R.M. and Puhakka J.A. (2006) *Desulfotomaculum thermosubterraneum* sp. nov., a thermophilic sulfate-reducer isolated from an underground mine located in a geothermally

- active area. *International Journal of Systematic and Evolutionary Microbiology*, **56**(11), 2603–2608, <https://doi.org/10.1099/ijs.0.64439-0>.
- Kappler A., Bryce C., Mansor M., Lueder U., Byrne J.M. and Swanner E.D. (2021) An evolving view on biogeochemical cycling of iron. *Nature Reviews Microbiology*, **19**(6), 360–374.
- Khan I.U., Habib N., Xiao M., Li M.-M., Xian W.-D., Hejazi M.S., Tarhriz V., Zhi X.-Y. and Li W.-J. (2019) *Rhodobacter thermarum* sp. nov., a novel phototrophic bacterium isolated from sediment of a hot spring. *Antonie van Leeuwenhoek*, **112**(6), 867–875, <https://doi.org/10.1007/s10482-018-01219-7>.
- Kim H., Stinchcomb G. and Brantley S.L. (2017) Feedbacks among O₂ and CO₂ in deep soil gas, oxidation of ferrous minerals, and fractures: A hypothesis for steady-state regolith thickness. *Earth and Planetary Science Letters*, **460**, 29–40.
- Klein F., Tarnas J.D. and Bach W. (2020) Abiotic sources of molecular hydrogen on Earth. *Elements: An International Magazine of Mineralogy, Geochemistry, and Petrology*, **16**(1), 19–24.
- Kodama Y. and Watanabe K. (2004) *Sulfuricurvum kujiense* gen. nov., sp. nov., a facultatively anaerobic, chemolithoautotrophic, sulfur-oxidizing bacterium isolated from an underground crude-oil storage cavity. *International Journal of Systematic and Evolutionary Microbiology*, **54**(6), 2297–2300.
- Krone L.V., Hampl F.J., Schwerdheim C., Bryce C., Ganzert L., Kitte A., Übernickel K., Dielforder A., Aldaz Cifuentes S.R. and Osés-Pedraza R. (2021a) Physical and geochemical data on a drill core from the semi-arid Coastal Cordillera, Chile. GFZ Data Services, Potsdam, <https://doi.org/10.5880/GFZ.3.3.2021.002>.
- Krone L.V. et al. (2021b) Deep weathering in the semi-arid Coastal Cordillera, Chile. *Scientific Reports*, **11**(1), 13057, <https://doi.org/10.1038/s41598-021-90267-7>.
- Krumholz L.R., McKinley J.P., Ulrich G.A. and Suflita J.M. (1997) Confined subsurface microbial communities in Cretaceous rock. *Nature*, **386**(6620), 64–66, <https://doi.org/10.1038/386064a0>.
- Kurtzer G.M., Sochat V. and Bauer M.W. (2017) Singularity: Scientific containers for mobility of compute. *PLOS One*, **12**(5), e0177459.
- Lalonde K., Mucci A., Ouellet A. and Gélinas Y. (2012) Preservation of organic matter in sediments promoted by iron. *Nature*, **483**, 198, <https://doi.org/10.1038/nature10855>.
- LaRowe, D and Amend, J. (2014) Energetic constraints on life in marine deep sediments in: *Microbial Life of the Deep Biosphere* (J. Kallmeyer and D. Wagner, editors). De Gruyter, Berlin, Boston, 279–302.
- Lin L.-H. et al. (2006) Long-term sustainability of a high-energy, low-diversity crustal biome. *Science*, **314**(5798), 479–482, <https://doi.org/10.1126/science.1127376>.
- Liu J., Fu B., Yang H., Zhao M., He B. and Zhang X.-H. (2015) Phylogenetic shifts of bacterioplankton community composition along the Pearl Estuary: the potential impact of hypoxia and nutrients. *Frontiers in Microbiology*, **6**, 64.
- Lüdecke C., Reiche M., Eusterhues K., Nietzsche S. and Küsel K. (2010) Acid-tolerant microaerophilic Fe(II)-oxidizing bacteria promote Fe(III)-accumulation in a fen. *Environmental Microbiology*, **12**(10), 2814–2825.
- Lueder U., Druschel G., Emerson D., Kappler A. and Schmidt C. (2018) Quantitative analysis of O₂ and Fe²⁺ profiles in gradient tubes for cultivation of microaerophilic Iron (II)-oxidizing bacteria. *FEMS Microbiology Ecology*, **94**(2), fix177.
- Magot M., Ollivier B. and Patel B.K.C. (2000) Microbiology of petroleum reservoirs. *Antonie van Leeuwenhoek*, **77**(2), 103–116, <https://doi.org/10.1023/A:1002434330514>.
- Mahmoud F.M., Kusari S., Kublik S.B., Siani R., Zühlke S., Radl V., Mahnkopp-Dirks F. and Schloter M. (2023) Draft genome sequence of the bacterial endophyte *Priestia megaterium* B1, isolated from roots of apple (*Malus domestica*). *Microbiology Resource Announcements*, **12**(6), e01172–01122, <https://doi.org/10.1128/mra.01172-22>.
- Martin M. (2011) Cutadapt removes adapter sequences from high-throughput sequencing reads. *EMBnet. Journal*, **17**(1), 10–12.
- McIlroy S.J., Kirkegaard R.H., McIlroy B., Nierychlo M., Kristensen J.M., Karst S.M., Albertsen M. and Nielsen P.H. (2017) MiDAS 2.0: an ecosystem-specific taxonomy and online database for the organisms of wastewater treatment systems expanded for anaerobic digester groups. *Database*, **2017**, bax016.
- Ministerio de Obras Públicas (2016) *Información oficial hidrometeorológica y de calidad de aguas en línea*. DGA (Dirección General de Aguas), Santiago de Chile, Chile.
- Minyard M.L., Bruns M.A., Liermann L.J., Buss H.L. and Brantley S.L. (2012) Bacterial associations with weathering minerals at the regolith-bedrock interface, Luquillo Experimental Forest, Puerto Rico. *Geomicrobiology Journal*, **29**(9), 792–803.
- Mitchell T.M. and Faulkner D.R. (2009) The nature and origin of off-fault damage surrounding strike-slip fault zones with a wide range of displacements: A field study from the Atacama fault system, northern Chile. *Journal of Structural Geology*, **31**(8), 802–816, <https://doi.org/10.1016/j.jsg.2009.05.002>.
- Moser D.P. et al. (2003) Temporal shifts in the geochemistry and microbial community structure of an ultradeep mine borehole following isolation. *Geomicrobiology Journal*, **20**(6), 517–548, <https://doi.org/10.1080/713851170>.
- Murray J., Clément A., Fritz B., Schmittbuhl J., Bordmann V. and Fleury J.M. (2020) Abiotic hydrogen generation from biotite-rich granite: A case study of the Soultz-sous-Forêts geothermal site, France. *Applied Geochemistry*, **119**, 104631.
- Napieralski S.A., Buss H.L., Brantley S.L., Lee S., Xu H. and Roden E.E. (2019) Microbial chemolithotrophy mediates oxidative weathering of granitic bedrock. *Proceedings of the National Academy of Sciences*, **116**(52), 26394–26401.
- Napieralski S.A., Fang Y., Marcon V., Forsythe B., Brantley S.L., Xu H. and Roden E.E. (2022) Microbial chemolithotrophic oxidation of pyrite in a subsurface shale weathering environment: Geologic considerations and potential mechanisms. *Geobiology*, **20**(2), 271–291.
- Oeser R.A., Stronck N., Moskwa L.-M., Bernhard N., Schaller M., Canessa R., van den Brink L., Köster M., Brucker E. and Stock S. (2018) Chemistry and microbiology of the Critical Zone along a steep climate and vegetation gradient in the Chilean Coastal Cordillera. *Catena*, **170**, 183–203.
- Oeser R.A. and von Blanckenburg F. (2020) Do degree and rate of silicate weathering depend on plant productivity? *Biogeosciences*, **17**(19), 4883–4917, <https://doi.org/10.5194/bg-17-4883-2020>.
- Ollivier B., Cayol J.-L. and Fauque G. (2007) Sulphate-reducing bacteria from oil field environments and deep-sea hydrothermal vents. Pp. 305–328 in *Sulphate-Reducing Bacteria: Environmental and Engineered Systems* (L.L. Barton and W.A. Hamilton, editors). Cambridge University Press, Cambridge.
- Onstott T.C., Ehlmann B.L., Sapers H., Coleman M., Ivarsson M., Marlow J.J., Neubeck A. and Niles P. (2019) Paleo-rock-hosted life on Earth and the search on Mars: a review and strategy for exploration. *Astrobiology*, **19**(10), 1230–1262.
- Osburn M.R., LaRowe D.E., Momper L.M. and Amend J.P. (2014) Chemolithotrophy in the continental deep subsurface: Sanford Underground Research Facility (SURF), USA. *Frontiers in Microbiology*, **5**(610), <https://doi.org/10.3389/fmicb.2014.00610>.
- Pedersen K. (1997) Microbial life in deep granitic rock. *FEMS Microbiology Reviews*, **20**(3–4), 399–414.
- Peiffer S., Maisch M., Kappler A., Schmidt C., Mansor M., Obst M. and Frei S. (2024) Kinetic constraints for the formation of microniches for microaerophilic Fe(II) oxidation. *Geochimica et Cosmochimica Acta*, **364**, 211–223, <https://doi.org/10.1016/j.gca.2023.11.006>.
- Perez J.R., Banwart S.A. and Puigdomenech I. (2005) The kinetics of O₂ (aq) reduction by structural ferrous iron in naturally occurring ferrous silicate minerals. *Applied Geochemistry*, **20**(11), 2003–2016.
- Picard A., Kappler A., Schmid G., Quaroni L. and Obst M. (2015) Experimental diagenesis of organo-mineral structures formed by microaerophilic Fe(II)-oxidizing bacteria. *Nature Communications*, **6**(1), 6277.
- Quast C., Pruesse E., Yilmaz P., Gerken J., Schweer T., Yarza P., Peplies J. and Glöckner F.O. (2012) The SILVA ribosomal RNA gene database project: improved data processing and web-based tools. *Nucleic Acids Research*, **41**(D1), D590–D596.
- Raiswell R., Canfield D.E. and Berner R.A. (1994) A comparison of iron extraction methods for the determination of degree of pyritisation and the recognition of iron-limited pyrite formation. *Chemical Geology*, **111**(1), 101–110, [https://doi.org/10.1016/0009-2541\(94\)90084-1](https://doi.org/10.1016/0009-2541(94)90084-1).
- Riebe C.S., Hahm W.J. and Brantley S.L. (2017) Controls on deep critical zone architecture: a historical review and four testable hypotheses. *Earth Surface Processes and Landforms*, **42**(1), 128–156, <https://doi.org/10.1002/esp.4052>.

- Roden E.E. and Zachara J.M. (1996) Microbial reduction of crystalline iron(III) oxides: Influence of oxide surface area and potential for cell growth. *Environmental Science & Technology*, **30**(5), 1618–1628, <https://doi.org/10.1021/es9506216>.
- Ross A.M., Peoples L.M., Bilbrey E.M. and Church M.J. (2022) Draft metagenome-assembled genomes from methane-rich Echo Lake, Montana. *Microbiology Resource Announcements*, **11**(2), e0111221, <https://doi.org/10.1128/mra.01112-21>.
- Samuels T., Bryce C., Landenmark H., Marie-Loudon C., Nicholson N., Stevens A.H. and Cockell C. (2020) Microbial weathering of minerals and rocks in natural environments. Pp. 59–79 in *Biogeochemical cycles: Ecological drivers and environmental impact* (K. Dontsova, Z. Balogh-Brunstad, G. Le Roux, editors). AGU and WILEY, Washington D.C. and Hoboken.
- Sato M., Sutton A.J. and McGee K.A. (1984) Anomalous hydrogen emissions from the San Andreas fault observed at the Cienega Winery, central California. *Pure and Applied Geophysics*, **122**(2), 376–391, <https://doi.org/10.1007/BF00874606>.
- Scheibe A., Sierra C.A. and Spohn M. (2023) Recently fixed carbon fuels microbial activity several meters below the soil surface. *Biogeosciences*, **20**(4), 827–838, <https://doi.org/10.5194/bg-20-827-2023>.
- Schröder K.-H., Naumann L., Kroppenstedt R. and Reischl U. (1997) *Mycobacterium hassiacum* sp. nov., a new rapidly growing thermophilic mycobacterium. *International Journal of Systematic Bacteriology*, **47**(1), 86–91.
- Shelobolina E., Xu H., Konishi H., Kukkadapu R., Wu T., Blöthe M. and Roden E. (2012) Microbial lithotrophic oxidation of structural Fe(II) in biotite. *Applied and Environmental Microbiology*, **78**(16), 5746–5752, <https://doi.org/10.1128/aem.01034-12>.
- Sidhu P., Gilkes R., Cornell R., Posner A. and Quirk J. (1981) Dissolution of iron oxides and oxyhydroxides in hydrochloric and perchloric acids. *Clays and Clay Minerals*, **29**, 269–276.
- Spring S. et al. (2012) Complete genome sequence of the sulfate-reducing firmicute *Desulfotomaculum ruminis* type strain (DLT). *Standards in Genomic Sciences*, **7**(2), 304–319, <https://doi.org/10.4056/sigs.3226659>.
- Straub D., Blackwell N., Langarica-Fuentes A., Peltzer A., Nahnsen S. and Kleindienst S. (2020) Interpretations of environmental microbial community studies are biased by the selected 16S rRNA (gene) amplicon sequencing pipeline. *Frontiers in Microbiology*, **11**, 550420.
- Straub K.L., Kappler A. and Schink B. (2005) Enrichment and isolation of ferric-iron-and humic-acid-reducing bacteria. *Methods in Enzymology*, **397**, 58–77.
- Suzuki S., Ishii S., Hoshino T., Rietze A., Tenney A., Morrill P.L., Inagaki F., Kuenen J.G. and Neelson K.H. (2017) Unusual metabolic diversity of hyper-alkaliphilic microbial communities associated with subterranean serpentinization at The Cedars. *The ISME Journal*, **11**(11), 2584–2598.
- Takamiya H., Kouduka M. and Suzuki Y. (2021) The deep rocky biosphere: new geomicrobiological insights and prospects. *Frontiers in Microbiology*, **12**, 785743.
- Team R.C. (2024) R: A language and environment for statistical computing. R Foundation for Statistical Computing. National Institute of Informatics, Tokyo.
- Trichandi R., Bauer K., Ryberg T., Scherler D., Bataille K. and Krawczyk C.M. (2022) Combined seismic and borehole investigation of the deep granite weathering structure – Santa Gracia Reserve case in Chile. *Earth Surface Processes and Landforms*, **47**(14), 3302–3316, <https://doi.org/10.1002/esp.5457>.
- Übernickel K., Ehlers T.A., Ershadi M.R., Paulino L., Fuentes Espoz J.-P., Maldonado A., Osés-Pedraza R. and von Blanckenburg F. (2020) Time series of meteorological station data in the EarthShape study areas in the Coastal Cordillera, Chile GFZ Data Services, Potsdam, <https://doi.org/10.5880/FID-GEO.2020.043>.
- Voelz J.L., Johnson N.W., Chun C.L., Arnold W.A. and Penn R.L. (2019) Quantitative dissolution of environmentally accessible iron residing in iron-rich minerals: A review. *ACS Earth and Space Chemistry*, **3**(8), 1371–1392.
- Walter X.A., Picazo A., Miracle M.R., Vicente E., Camacho A., Aragno M. and Zopfi J. (2014) Phototrophic Fe(II)-oxidation in the chemocline of a ferruginous meromictic lake. *Frontiers in Microbiology*, **5**, 713.
- Wang P., Xiao X., Zhang H. and Wang F. (2008) Molecular survey of sulphate-reducing bacteria in the deep-sea sediments of the west Pacific Warm Pool. *Journal of Ocean University of China*, **7**(3), 269–275, <https://doi.org/10.1007/s11802-008-0269-9>.
- Warnecke F., Amann R. and Pernthaler J. (2004) Actinobacterial 16S rRNA genes from freshwater habitats cluster in four distinct lineages. *Environmental Microbiology*, **6**(3), 242–253.
- Weckmann U., Bauer K., Krawczyk C., Kück J., Übernickel K. and von Blanckenburg F. (2020) Geophysical borehole logging data from Santa Gracia, Chile. GFZ Data Services, Potsdam, <https://doi.org/10.5880/GFZ.2.7.2020.001>.
- White A.F. and Yee A. (1985) Aqueous oxidation-reduction kinetics associated with coupled electron-cation transfer from iron-containing silicates at 25°C. *Geochimica et Cosmochimica Acta*, **49**(5), 1263–1275.
- Wickham H. (2016) Programming with ggplot2. Pp. 241–253 in *ggplot2: Elegant Graphics for Data Analysis* (H. Wickham, editor). Springer, Cham.
- Widdel F., Schnell S., Heising S., Ehrenreich A., Assmus B. and Schink B. (1993) Ferrous iron oxidation by anoxygenic phototrophic bacteria. *Nature*, **362**(6423), 834–836, <https://doi.org/10.1038/362834a0>.
- Xian W.-D., Liu Z.-T., Li M.-M., Liu L., Ming Y.-Z., Xiao M., Salam N. and Li W.-J. (2020) *Rhodobacter flagellatus* sp. nov., a thermophilic bacterium isolated from a hot spring. *International Journal of Systematic and Evolutionary Microbiology*, **70**(3), 1541–1546, <https://doi.org/10.1099/ijsem.0.003929>.
- Xiao D., Brantley S.L. and Li L. (2021) Vertical connectivity regulates water transit time and chemical weathering at the Hillslope scale. *Water Resources Research*, **57**(8), e2020WR029207, <https://doi.org/10.1029/2020WR029207>.
- Yasawong M., Areekit S., Pakpitchareon A., Santiwatanakul S. and Chansiri K. (2011) Characterization of thermophilic halotolerant *Aeribacillus pallidus* TD1 from Tao dam hot spring, Thailand. *International Journal of Molecular Sciences*, **12**(8), 5294–5303.
- Zhuang K., Izallalen M., Mouser P., Richter H., Risso C., Mahadevan R. and Lovley D.R. (2011) Genome-scale dynamic modeling of the competition between *Rhodospirillum rubrum* and *Geobacter* in anoxic subsurface environments. *The ISME Journal*, **5**(2), 305–316, <https://doi.org/10.1038/ismej.2010.117>.
- Zuur A.F., Ieno E.N., Walker N.J., Saveliev A.A. and Smith G.M. (2009) *Mixed effects models and extensions in ecology with R*. Springer, New York.